Dear Author,

Please, note that changes made to the HTML content will be added to the article before publication, but are not reflected in this PDF.

Note also that this file should not be used for submitting corrections.

AUTHOR QUERY FORM

ELSEVIER	**Journal: GCA** **Article Number: 9215**	**Please e-mail your responses and any corrections to:** **E-mail: corrections.essd@elsevier.sps.co.in**

Dear Author,

Please check your proof carefully and mark all corrections at the appropriate place in the proof (e.g., by using on-screen annotation in the PDF file) or compile them in a separate list. Note: if you opt to annotate the file with software other than Adobe Reader then please also highlight the appropriate place in the PDF file. To ensure fast publication of your paper please return your corrections within 48 hours.

For correction or revision of any artwork, please consult http://www.elsevier.com/artworkinstructions.

Any queries or remarks that have arisen during the processing of your manuscript are listed below and highlighted by flags in the proof. Click on the 'Q' link to go to the location in the proof.

Location in article	Query / Remark: click on the Q link to go Please insert your reply or correction at the corresponding line in the proof
Q1	Your article is registered as a regular item and is being processed for inclusion in a regular issue of the journal. If this is NOT correct and your article belongs to a Special Issue/Collection please contact a.mutale1@elsevier.com immediately prior to returning your corrections.
Q2	Please confirm that given name(s) and surname(s) have been identified correctly.
Q3	Please check the address for the corresponding author 'Y. Mei' that has been added here, and correct if necessary.
Q4	The citations 'Bethke et al. (2008), Beret et al. (2008), Becke (1998), Gammons et al. (1995), Mountain and Wood (1988), Resat (1993), Barnes et al. (2004), Sassani et al. (1990, 1998)' have been changed to 'Bethke (2008), Beret et al. (2008a,b), Becke (1993), Gammons (1995), Wood and Mountain (1991), Resat and Mihaly (1993), Barnes (2004), Sassani and Shock (1990, 1998)' to match the author name/date in the reference list. Please check, and correct if necessary.
Q5	References 'Tian et al. (2013), Cabral et al. (2003), Boily and Seward (2005)' are cited in the text but not provided in the reference list. Please provide them in the reference list or delete these citations from the text.
Q6	'Section 3.3' was not found in this document. Please check.
Q7	This section comprises reference that occur in the reference list but not in the body of the text. Please position each reference in the text or, alternatively, delete it. Any reference not dealt with will be retained in this section.
Q8	One or more sponsor names may have been edited to a standard format that enables better searching and identification of your article. Please check and correct if necessary.
Q9	The country names of the Grant Sponsors are provided below. Please check and correct if necessary. 'Australian Research Council' - 'Australia', 'Minerals and Energy Research Institute of Western Australia' - 'Australia'.

Please check this box if you have no corrections to make to the PDF file ☐

Thank you for your assistance.

Available online at www.sciencedirect.com
ScienceDirect
Geochimica et Cosmochimica Acta xxx (2015) xxx–xxx
Geochimica et Cosmochimica Acta
www.elsevier.com/locate/gca

Palladium complexation in chloride- and bisulfide-rich fluids: Insights from *ab initio* molecular dynamics simulations and X-ray absorption spectroscopy

Yuan Mei[a,b,*], Barbara Etschmann[a], Weihua Liu[b], David M. Sherman[c], Stephen J. Barnes[d], Marco L. Fiorentini[e], Terry M. Seward[f], Denis Testemale[g], Joël Brugger[a,*]

[a] *School of Earth, Atmosphere and the Environment, Monash University, Clayton, VIC 3800, Australia*
[b] *CSIRO Mineral Resources Flagship, Clayton, VIC 3168, Australia*
[c] *School of Earth Sciences, University of Bristol, Bristol BS8 1RJ, UK*
[d] *CSIRO Mineral Resources Flagship, Kensington, WA 6151, Australia*
[e] *Australian Research Council Centre of Excellence for Core to Crust Fluid Systems, The University of Western Australia, Perth, Australia*
[f] *Victoria University of Wellington, New Zealand*
[g] *FAME beamline, ESRF, 38043 Grenoble, France*

Received 16 December 2014; accepted in revised form 3 April 2015; available online xxxx

Abstract

Palladium (Pd) is the most mobile element of the platinum group elements (PGE) in hydrothermal fluids. The characterization of the nature and stability of Pd(II) complexes in geofluids is essential in understanding the formation of hydrothermal PGE deposits and the remobilization of PGE during hydrothermal and metamorphic overprints of magmatic deposits. However, the aqueous speciation of this metal in a range of geologically relevant conditions remains controversial. A number of experimental studies of Pd solubility and speciation in hydrothermal fluids suggest that chloride and bisulfide are the major ligands responsible for carrying Pd as Pd(II)–Cl and Pd(II)–HS complexes, but different experimental studies predicted different predominant chloride and bisulfide complexes and their relative strengths. Hence, we conducted *ab initio* molecular dynamics (MD) simulations to predict the speciation of Pd–Cl and Pd–HS complexes at 300 °C. The simulations predicted that all complexes share fourfold square-planar structures, which is consistent with X-ray absorption spectroscopy measurements of Pd(II) in chloride-rich solutions. The stability constants for the stepwise formation of Pd(II)–Cl and Pd(II)–HS complexes were determined using thermodynamic integration. The predicted formation constants of Pd(II)–Cl complexes show excellent agreement (within ~1 order of magnitude for $PdCl^+$, within 0.3 for $PdCl_{2(aq)}$ and $PdCl_3^-$, within 0.1 for $PdCl_4^{2-}$) with the recent experimental study of Tagirov et al. (2013). However, our results suggest that the $Pd(HS)_4^-$ complex predominates in HS^--rich hydrothermal fluids, whereas interpretation of previous experimental studies neglected this species. Modeling of Pd solubility in chloride- and sulfur-rich hydrothermal fluids demonstrated that Pd is mainly carried as the $Pd(HS)_4^{2-}$ hydrosulfide complex at neutral-alkaline and reduced (pyrite/pyrrhotite stable) conditions, and as the $PdCl_4^{2-}$ chloride complex at acidic and oxidized conditions. At 300 °C, significant Pd mobility at ppb level as Pd bisulfide complexes is predicted under fluid-buffered conditions (e.g., pH ~7 to 8, near HS^-/H_2S(aq) pH buffer), but only limited Pd solubility is predicted under rock-buffered conditions (e.g., pH ~4 to 5, quartz–feldspar–muscovite buffer).
© 2015 Published by Elsevier Ltd.

* Corresponding authors at: School of Earth, Atmosphere and the Environment, Monash University, Clayton, VIC 3800, Australia (Y. Mei).
E-mail addresses: yuan.mei@monash.edu, yuan.mei@csiro.au (Y. Mei), joel.brugger@monash.edu (J. Brugger).

http://dx.doi.org/10.1016/j.gca.2015.04.009
0016-7037/© 2015 Published by Elsevier Ltd.

UNCORRECTED PROOF

1. INTRODUCTION

Aqueous metal speciation plays an important role in controlling metal transport and deposition in hydrothermal fluids in both natural and man-made environments (Seward and Driesner, 2004; Brugger et al., 2010). Characterizing the speciation and solubility of platinum group elements (PGE) in hydrothermal fluids is useful in understanding and critically evaluating (1) the formation of hydrothermal PGE deposits (e.g., Boudreau et al., 1986; Mernagh et al., 1994; Farrow and Watkinson, 1996; Wood, 2002); (2) the significance of PGE as petrogenetic indicators in hydrothermal settings (e.g., porphyry copper deposits; Xiong and Wood, 2000); and (3) the mobility of PGE during hydrothermal and/or metamorphic overprint of magmatic Ni-Cu-PGE deposits, leading to the formation of secondary enrichments or alteration halos that may enlarge the footprint of these deposits (e.g., Willmore et al., 2000; Barnes, 2004; Barnes and Liu, 2012; Djon and Barnes, 2012; Le Vaillant et al., 2014).

The distribution of PGE, in particular palladium, has long been recognized as a marker for ore-forming processes (e.g., Fiorentini et al., 2010; Barnes et al., 2013; Locmelis et al., 2013) and hydrothermal alteration of magmatic nickel deposits (e.g., Keays and Davison, 1976; Le Vaillant et al., 2014). Recently, Barnes and Liu (2012) observed that magmatic Pd/Pt ratios were preserved within metamorphosed komatiite-hosted Ni ores where the S-contents were low, but varied greatly around S-rich ore bodies. Based on available thermodynamic data, they suggested that this pattern of Pd mobility was due to the fact that bisulfide complexes, rather than chloride complexes, dominate Pd speciation at $T \geqslant 300$ °C in moderately reduced, S-rich aqueous fluids in the Earth's crust.

Palladium is the most mobile PGE element in geofluids (Cabral et al., 2012; Tagirov et al., 2013). The thermodynamic models and properties for aqueous PGE complexes have been estimated by a number of studies (Wood et al., 1989; Sassani and Shock, 1990, 1998; Wood and Mountain, 1991). Chlorine and sulfur are the main elements involved in the complexing of metals in natural hydrothermal fluids (e.g., Seward and Barnes, 1997). Consequently, a number of experimental studies have investigated Pd speciation and solubility in chloride and hydrosulfide solutions under hydrothermal conditions up to 700 °C (Hsu et al., 1991; Wood et al., 1992; Gammons et al., 1992, 1993; Pan and Wood, 1994; Gammons, 1995; Seward et al., 2002; Boily and Seward, 2005, 2007; Tagirov and Baranova, 2009; Tagirov et al., 2013; Bazarkina et al., 2014).

Despite this extensive amount of work, large discrepancies still exist among different studies and the resulting thermodynamic models. For example, Xiong and Wood (2000) noted that the Pd and Pt solubility calculated using the available thermodynamic properties are several orders of magnitudes lower than expected from mass balance considerations and from experimental values for porphyry copper environments (350–500 °C). Two main groups have provided extensive experimental work, with the results and preferred thermodynamic properties summarized in Wood et al. (1992) and Tagirov et al. (2013), respectively. In general, the formation constants ($\log \beta_n$) for the Pd chloride complexes ($PdCl_n^{2-n}$) up to 300 °C and the solubility predicted by both models in chloride brines are in reasonable agreement (predicted solubilities within one order of magnitude). However, at 300 °C the formation constant of $PdCl_4^{2-}$, a dominant complex in moderately saline fluids, are about two orders of magnitude higher according to Tagirov et al. (2013) than in the earlier study of Wood et al. (1992). The situation is much worse for Pd–bisulfide complexes, due to the scarcity of experimental data and the variety of experimental challenges encountered. Both groups proposed different predominating Pd–HS species. Consequently, if Pd solubilities in sulfur-rich solutions calculated on the basis of the earlier experimental studies by Gammons and Bloom (1993) and Pan and Wood (1994) are in reasonable agreement, those predicted using the data of Tagirov and Baranova (2009) are several orders of magnitude lower. Furthermore, the absence of $Pd(HS)_4^{2-}$ in the interpretation of experimental data (Wood et al., 1992; Tagirov et al., 2013) poses an interesting (geo)chemical conundrum, since the $PdCl_4^{2-}$ complex is acknowledged by all studies to be the most important complex in chloride brines (see also Bazarkina et al., 2014).

These discrepancies severely hinder our understanding of PGE mobility in hydrothermal fluids and the reliability of the predictions of numerical reactive transport modeling. For example, the conclusion of Barnes and Liu (2012) that the disturbance of Pd/Pt ratios in komatiite-hosted massive sulfide ores is due to bisulfide complexing of Pd during hydrothermal overprint is not consistent with the model of Tagirov et al. (2013); this illustrates that even first order predictions depend on the choice of the model. Consequently, it is desirable to use alternative experimental and/or theoretical approaches to investigate PGE speciation and solubility in hydrothermal fluids to confirm the available experimental data.

The geometrical properties of Pd–Cl complexes have been investigated by X-ray absorption spectroscopy (XAS) (Seward et al., 2002; Seward and Driesner, 2004; Bazarkina et al., 2014). Several theoretical studies have also investigated the structure of Pd(II) complexes using *ab initio* calculations on gas-phase molecules (Boily and Seward, 2005; Boily et al., 2007). Metal–ligand interactions (e.g., bond lengths) are generally well reproduced using Density Functional Theory (DFT) with current generalized-gradient exchange–correlation functionals. *Ab initio* MD was employed extensively to investigate the hydration of Pd^{2+} ions (e.g., Martínez et al., 2004; Hofer et al., 2007; Beret et al., 2008a,b; Bowron et al., 2011; Vidossich et al., 2011). The studies listed above found good agreement between the predicted and experimental structural properties investigated. The difference of Pd–O bond distances between theoretical studies and experiments (e.g., 2.01–2.04 Å from experiments versus 2.052/2.065 Å from *ab initio* calculation with B3LYP exchange–correlation functional, Boily and Seward, 2005) are inline with the expected accuracy of the DFT approach (e.g., Bühl et al., 2006).

Using *ab initio* MD simulations, we can also explore the thermodynamics of metal complexation at hydrothermal

UNCORRECTED PROOF

Please cite this article in press as: Mei Y., et al. Palladium complexation in chloride- and bisulfide-rich fluids: Insights from *ab initio* molecular dynamics simulations and X-ray absorption spectroscopy. *Geochim. Cosmochim. Acta* (2015), http://dx.doi.org/10.1016/j.gca.2015.04.009

conditions (e.g., Mei et al., 2013a, 2014, 2015). In principle, if the ion/ligand exchange time is within the time scale of *ab initio* MD simulation (pico-seconds), the relative stability constants of different complexes can be derived from the statistical proportion of different species along the simulation time, as demonstrated for example for the ion association between $CuCl_2^-$ and Na^+ (Mei et al., 2014). However, for most complexation reactions between metal and ligand (e.g., Cl^-, HS^-), the ligand residence time (e.g., ~300 μs for Zn(II)–Cl at 25 °C, Sharps et al., 1993) is far beyond the accessible ~100 ps timescale of *ab initio* MD simulations (see discussion in Mei et al., 2015). Using thermodynamic integration, however, we can calculate the free energy of complex formation in the course of a constrained molecular dynamics simulation. The most straightforward approach is to integrate the time-averaged forces along a reaction path corresponding to the metal–ligand interatomic distances. This approach was used successfully for complexes in the Cu(I)–HS–Cl (Mei et al., 2013a) and Zn(II)–Cl systems (Mei et al., 2015). In the case of Cu(I), the calculated thermodynamic properties for the ligand exchange reactions compared well with the existing, well constrained experimentally-derived properties. In the case of Zn(II), it was possible to derive a new thermodynamic model based on the predictions from *ab initio* MD, which is consistent with most existing (and previously assumed to be conflicting) experimental data. Thermodynamic integration hence provides an independent and complementary approach to investigate the thermodynamic properties of transition metal complexes under hydrothermal conditions.

The goal of this study is to use *ab initio* MD simulations to provide a speciation model for the Pd–Cl–HS system and to determine the thermodynamic properties for the predominant palladium chloride and hydrosulfide complexes. These studies were complemented by investigations into the speciation of Pd in chloride and sulfide systems at temperatures to 350 °C at 800 bar via *in-situ* X-ray absorption spectroscopy.

2. METHODOLOGY

2.1. *Ab initio* molecular dynamics simulations

Ab initio MD simulations were conducted using the Car–Parrinello (CP) molecular dynamics code CPMD (Car and Parrinello, 1985). Car–Parrinello molecular dynamics simulations implement density functional theory using a plane-wave basis set and pseudo-potentials for the core electrons plus the nucleus. The BLYP exchange–correlation functional was employed with a cutoff of gradient correction 5×10^{-8} (Lee et al., 1988; Becke, 1988). BLYP functional provides a good description of water properties such as O–O interaction, angular distributions, coordination numbers and H-Bond statistics (Lin et al., 2012). Plane-wave cutoffs of 80 Ry (1088.46 eV) were used together with Martins–Troullier pseudo-potentials in the CPMD package generated using the valence electron configuration $4d^9 5s^1$ for Pd (Troullier and Martins, 1991). Molecular dynamics simulations were conducted in the NVT ensemble. A time-step of 3 a.u. (0.073 fs) was used to stabilize the simulations. Temperatures were controlled by the Nosé thermostat for both ions and electrons. The target fictitious kinetic energies of 0.032 were obtained by taking the converged value of a 10,000-steps simulation with no defined Nosé thermostat for electrons. A fictitious electron mass of 400 a.u. (3.644×10^{-28} kg) was used to obtain convergence of the energy of the total CP-Hamiltonians. The initial atomic configurations of each simulation were generated by classical MD using the SPC/E potential for water and approximate pair potentials derived from finite cluster calculations for Pd–O, Pd–Cl and Pd–S (Berendsen et al., 1987; Smith and Dang, 1994).

Ab initio molecular dynamics simulations of Pd(II)–Cl complexation were conducted at 125 °C, 14 bar (vapor-saturated pressure) and 300 °C, 500 bar with 1 Pd^{2+}, 2 Na^+, 4 Cl^- and 55 H_2O in the simulation box corresponding to bulk chloride concentrations of 4 molal (Table 1). Periodic boundary conditions were used to eliminate surface effects. The fluid densities were chosen to correspond to the equation of state of NaCl fluids at the same ionic strength at the pressure and temperature of interest (Driesner, 2007; Driesner and Heinrich, 2007). To investigate the stability of different Pd–Cl complexes, at each temperature, six *ab initio* MD simulations were performed with different initial configurations of $Pd(H_2O)_{4-n}Cl_n^{2-n}$ ($n = 0$, 1, 2, 3, 4). All simulations were run for more than 100,000 steps (7 ps). The hard Martins–Troullier pseudo-potential used in this study requires larger plane-wave cutoffs (80 Ry in this study) than the ultrasoft pseudo-potentials used in our earlier Cu(I) and Zn(II) studies (25 Ry; Mei et al., 2013a,b, 2015); consequently, the *ab initio* MD simulations in this study cost many more CPU hours (~2000 CPU hours per ps) than those using ultrasoft pseudo-potentials (330–520 CPU hours per ps). As discussed in Mei et al. (2013a), the size of the simulation boxes (172 atoms) and the simulation times (>7 ps) chosen in this study provide manageable computation times while enabling the simulation of realistic solution compositions. Similarly, *ab initio* MD simulations of Pd–HS complexation were conducted at 300 °C, 500 bar in a simulation box corresponding to fluids containing 4 molal HS^- (1 Pd^{2+}, 2 Na^+, 4 HS^- and 55 H_2O; Table 1), corresponding to alkaline conditions with pH > 7.1. The pH ranges were

Table 1
Solution composition, temperature, pressure and density of Pd(II)–Cl and Pd(II)–HS MD simulations.

Job no.	Solution composition	T (°C)	P (bar)	Box size (Å)	Density (g/cm^3)
1	1 Pd, 2 Na, 4 Cl and 55 H_2O	125	14	12.346	1.133
2	1 Pd, 2 Na, 4 Cl and 55 H_2O	300	500	13.102	0.949
3	1 Pd, 2 Na, 4 HS and 55 H_2O	300	500	13.102	0.942

UNCORRECTED PROOF

Please cite this article in press as: Mei Y., et al. Palladium complexation in chloride- and bisulfide-rich fluids: Insights from *ab initio* molecular dynamics simulations and X-ray absorption spectroscopy. *Geochim. Cosmochim. Acta* (2015), http://dx.doi.org/10.1016/j.gca.2015.04.009

evaluated by approximating the neutrality point of water (5.4) and pK_a of H_2S/HS^- from the HCh database at 300 °C, 500 bar (Shvarov and Bastrakov, 1999; Shvarov, 2008). The average distances for Pd–Cl, Pd–O and Pd–S were calculated and listed in Tables 2 and 3. We use Debye–Waller factors (σ^2) to characterize the disorder of the bond distances, as this allows for direct comparison with experimental measurements (Campbell et al., 1999).

2.2. *Ab initio* thermodynamic integration

Thermodynamic integration (Resat and Mihaly, 1993; Sprik and Ciccotti, 1998) was employed to evaluate the free energies of ligand exchange reactions for Pd(II) chloride and bisulfide complexes using a method similar to that described in Mei et al. (2013a, 2015). The method relies on measuring the work necessary to transform a (meta-)stable configuration (1) into (meta-)stable configuration (2). In this case, a study of ligand exchange reactions was achieved by constraining the Pd–ligand distance for one of the ligands in configuration (1) along a predefined path from equilibrium bond distance to no interaction. One example is discussed in detail in Section 3.2. At each constrained distance, the force required to maintain the Pd(II)–ligand distance was measured over a >5 ps *ab initio* MD simulation time (including 0.7 ps for initial stabilization), in order to sample the mean constrained force $f(r)$ at different configurations of the Pd–(Cl/HS) complexes and the surrounding solvent and salt molecules (Bühl et al., 2006, 2008). The free energy difference for the reaction of ligand exchange between the initial and final configurations were derived by integrating $f(r)$ with respect to the constrained distance r (Bühl et al., 2006, 2008; Sprik and Ciccotti, 1998):

$$\Delta_r A_{a\to b} = -\int_a^b \langle f(r)\rangle dr \quad (1)$$

As the simulations were conducted at constant volume, the obtained free energies are Helmholtz free energies ($\Delta_r A_{a\to b}$). To calculate the equilibrium constant of the

Table 2
Geometrical details of Pd(II)-Cl complexes by MD simulations.

T, *P*	Job no.	Simulation time (ps)	Initial structure	Final structure	Pd–Cl		Pd–O	
					R^* (Å)	σ^2_{Cl} (Å^2)	R^* (Å)	σ^2_{O} (Å^2)
125 °C 14 bar	1a	7.25	$Pd(H_2O)_6^{2+}$(ot)	$Pd(H_2O)_4^{2+}$(sq)	–	–	2.07(7)	0.004
							2.07(6)	0.004
							2.08(6)	0.004
							2.07(6)	0.004
	1b	11.6	$PdCl(H_2O)_3^+$(sq)	$PdCl(H_2O)_3^+$(sq)	2.37(7)	0.005	2.07(6) (cis)	0.003
							2.08(6) (cis)	0.003
							2.12(6) (trans)	0.004
	1c	7.25	$PdCl_2(H_2O)_2$(sq-cis)	$PdCl_2(H_2O)_2$(sq-cis)	2.38(7)	0.006	2.12(8)	0.007
					2.37(7)	0.005	2.11(8)	0.006
	1d	7.25	$PdCl_2(H_2O)_2$(sq-trans)	$PdCl_2(H_2O)_2$(sq-trans)	2.40(8)	0.006	2.08(7)	0.006
					2.40(7)	0.005	2.08(7)	0.004
	1e	10.87	$PdCl_3(H_2O)^-$(sq)	$PdCl_3(H_2O)^-$(sq)	2.40(8) (cis)	0.006	2.12(8)	0.006
					2.41(8) (cis)	0.007		
					2.38(7) (trans)	0.005		
	1f	10.15	$PdCl_4^{2-}$(sq)	$PdCl_4^{2-}$(sq)	2.41(8)	0.007	–	–
					2.42(8)	0.007		
					2.42(9)	0.008		
					2.41(8)	0.007		
300 °C 500 bar	2a	8.35	$PdCl(H_2O)_3^+$sq	$PdCl(H_2O)_3^+$ (sq)	2.37(8)	0.006	2.09(8)	0.007
							2.13(8)	0.006
							2.10(9)	0.008
	2b	8.01	$PdCl_2(H_2O)_2$(aq)(td)	$PdCl_2(H_2O)_2$(aq) (sq-cis)	2.37(8)	0.006	2.14(8)	0.006
					2.36(6)	0.004	2.14(9)	0.008
	2c	7.25	$PdCl_2(H_2O)_2$(aq)(sq-trans)	$PdCl_2(H_2O)_2$(aq) trans-sq$_{(Cl–Pd–Cl\ 169°)}$	2.42(13)	0.017	2.10(9)	0.009
					2.42(13)	0.017	2.10(8)	0.007
	2d	7.25	$PdCl_3(H_2O)^-$(sq)	$PdCl_3(H_2O)^-$ sq	2.42(10)	0.010	2.16(12)	0.014
					2.38(9)	0.007		
					2.42(9)	0.008		
	2e	9.07	$PdCl_4^{2-}$(sq)	$PdCl_4^{2-}$ sq	2.42(10)	0.009	–	–
					2.43(11)	0.011		
					2.43(9)	0.009		
					2.43(10)	0.009		

* The number in the () represent the standard deviation of average distances.

UNCORRECTED PROOF

Please cite this article in press as: Mei Y., et al. Palladium complexation in chloride- and bisulfide-rich fluids: Insights from *ab initio* molecular dynamics simulations and X-ray absorption spectroscopy. *Geochim. Cosmochim. Acta* (2015), http://dx.doi.org/10.1016/j.gca.2015.04.009

Table 3
Geometrical details of Pd(II)–HS complexes by MD simulations.

T, P, density	Job no.	Simulation time (ps)	Initial structure	Structure during MD simulation	Pd–S		Pd–O	
					R^* (Å)	σ^2_S (Å^2)	R^* (Å)	σ^2_O (Å^2)
300 °C 500 bar	3a	11.98	$Pd(H_2O)_6^{2+}$(ot)	$Pd(OH)(H_2O)_3^+$(sq) (7.23 ps) (Fig. 3a)	–	–	2.02(8) (O_1)	0.006
							2.12(9) (O_2)	0.008
							2.11(9)(O_3)	0.008
							2.16(12) (O_4)	0.014
				$Pd(OH)_2(H_2O)_2$ (3.60 ps) (Fig. 3b)			2.04(6) (O_1)	0.004
							2.03(6) (O_2)	0.004
							2.15(9) (O_3)	0.007
							2.16(9) (O_4)	0.009
	3b	8.43	$Pd(HS)(H_2O)_3^+$ td	$Pd(HS)(H_2O)_3^+$ sq (Fig. 3c)	2.39(10)	0.010	2.10(7) (O_1)	0.005
							2.11(8) (O_2)	0.007
							2.23(16) (O_3)	0.025
	3c	7.11	$Pd(HS)_2(H_2O)_2$(aq) td	$Pd(HS)_2(H_2O)_2$(aq)cis-sq (Fig. 3d)	2.38(9)	0.008	2.21(9)	0.007
					2.37(7)	0.005	2.22(10)	0.010
	3d	11.93	$Pd(HS)_2(H_2O)_2$(aq) trans-sq	$Pd(HS)_2(H_2O)_2$ (trans-sq) (5.30 ps)(Fig. 3e)	2.46(10)	0.011	2.12(10)	0.010
					2.46(10)	0.009	2.14(9)	0.009
				$[Pd(HS)_2(OH)(H_2O)]^-$ (trans-sq) (6.63 ps)(Fig. 3f)	2.46(9)	0.008	2.04(6) (O_1)	0.003
					2.46(9)	0.008	2.17(11) (O_2)	0.011
	3e	6.29	$Pd(HS)_3(H_2O)^-$ td	$Pd(HS)_3(H_2O)^-$ Sq (Fig. 3g)	2.38(8)	0.007	2.26(11)	0.013
					2.46(10)	0.011		
					2.46(11)	0.012		
	3f	7.24	$Pd(HS)_4^{2-}$ sq	$Pd(HS)_4^{2-}$ Sq (Fig. 3h)	2.47(10)	0.010	–	–
					2.48(10)	0.010		
					2.47(10)	0.009		
					2.47(9)	0.009		

* The number in the () represent the standard deviation of average distances.

ligand exchange reactions, the Gibbs free energies of reaction were approximated by assuming that the contribution of the pressure change for the reaction at constant V can be neglected (i.e., $\int_{P_0}^{P} dp \approx 0$ in Eq. 2)

$$\Delta_r G = \Delta_r A_{a\to b} + V \int_{P_0}^{P} dp, \quad (2)$$

where V is the volume of the simulation box.

The standard Gibbs free energies $\Delta_r G^{\Theta}$ for each reaction were obtained after activity and concentration corrections as in Mei et al. (2013a, 2015). Finally, the stepwise formation constants K^{Θ} were calculated from:

$$\Delta_r G^{\Theta} = -RT \ln K^{\Theta} \quad (3)$$

where R is the gas constant and T the temperature in Kelvin.

2.3. *In situ* X-ray absorption spectroscopy measurement and data processing

Deionised water and analytical grade chemicals $PdCl_2$ (99%), $PdBr_2$ (99%), PdS (99.9%), HCl (37 wt%), HBr (48 wt%), LiCl and NaCl, purchased from Sigma–Aldrich® were used without further treatment. Experimental solution compositions are given in Table 4. Palladium K-edge (24,350 eV) Extended X-ray absorption Fine Structure (EXAFS) spectra were measured at beamline 30-BM (FAME) at the European Synchrotron Radiation Facility (ESRF) in Grenoble, France. The ESRF is a 6.03 GeV ring and was operated in 7/8 multi-bunch mode with a maximum current of 200 mA. FAME is a bending magnet beam line with a double crystal Si(2 2 0) monochromator, and an energy resolution of 1.22 eV at the Pd K-edge (Proux et al., 2005a,b). The beam was focused to a FWHM of 300 × 800 μm^2. The incident and transmitted beam intensities, I_0 and I_1, were measured with Si diodes, and a Canberra 30 element solid-state fluorescence detector was used for detecting fluorescence data. The beam energy was calibrated with a Pd foil. The high temperature-high pressure cell developed by the "Laboratoire de Cristallographie" (CNRS) was used for XAS measurements of solutions up to supercritical conditions (Testemale et al., 2005). The cell consists of an external water-cooled high-pressure vessel equipped with three 1.5 mm thick beryllium windows enabling collection of fluorescence and transmission signals at a maximum pressure of ~800 bar. The sample was contained inside a glassy carbon tube with an internal diameter of 5 mm. The pressure was applied to the sample by two glassy carbon pistons, using helium as a pressure medium. The glassy carbon tube was placed inside a small cylindrical resistive heater; the heater and tube are then installed inside the high-pressure vessel. The temperature at the beam position was calibrated by measuring the density of pure water (Lemmon et al., 2000) by its X-ray absorption (e.g., Brugger et al., 2007; Etschmann et al., 2010; Liu et al., 2012).

UNCORRECTED PROOF

Table 4
Refined EXAFS parameters (n: number of ligand; r: bond length (Å); σ^2: Debye–Waller; χ^2_{red}: reduced chi-square.).

Solution	T, P	n_O, r_O (Å), σ^2_O (Å^2)	n_{Cl}, r_{Cl} (Å), σ^2_{Cl} (Å^2)	GOF, E_{0s}
Solution #1: 0.058 m $PdCl_2$ + 0.953 m HCl				
$2 \leqslant k \leqslant 12$ $1 \leqslant R \leqslant 5$	30 °C, 800 bar	Max n_O ~0.3(3), effectively no Pd–O	$n_{Cl} = 4$ (fix) $r_{Cl} = 2.305(2)$ Å $\sigma^2_{Cl} = 0.0010(3)$ Å^2	$\chi^2_{red} = 138$ $E_0 = 6.1(3)$
$2 \leqslant k \leqslant 12$ $1 \leqslant R \leqslant 5$	70 °C, 800 bar		$n_{Cl} = 4$ (fix) $r_{Cl} = 2.305(2)$ Å $\sigma^2_{Cl} = 0.0027(3)$ Å^2	
$2 \leqslant k \leqslant 10$ $1 \leqslant R \leqslant 5$	130 °C, 800 bar		$n_{Cl} = 4$ (fix) $r_{Cl} = 2.305(2)$ Å $\sigma^2_{Cl} = 0.0035(5)$ Å^2 $r_{Pd–Cl–Pd–Cl–Pd} = 2 \times rCl$ $\sigma^2_{Cl\ Pd–C–Pd–Cl–Pd} = \sigma^2_{Cl}$	
Solution #2: 0.008 m $PdCl_2$ + 5.065 m $HClO_4$				
$2 \leqslant k \leqslant 12$ $1 \leqslant R \leqslant 5$	Ambient	$n_O = 2$* $r_O = 2.022(9)$ Å σ^2_O§ $= 0.0007(5)$ Å^2 $r_{Pd–O–Pd–O–Pd} = 2 \times rO$ $\sigma^2_{O\ Pd–O–Pd–O–Pd} = \sigma^2_O$	$n_{Cl} = 2$* $r_{Cl} = 2.274(5)$ Å $\sigma^2_{Cl} = 0.0007(5)$ Å^2 $r_{Pd–Cl–Pd–Cl–Pd} = 2 \times rCl$ $\sigma^2_{Cl\ Pd–Cl–Pd–Cl–Pd} = \sigma^2_{Cl}$ $r_{Pd-Cl-Cl-Pd} = 2$ x rCl $\sigma^2_{Cl\ Pd-Cl-Cl-Pd} = \sigma^2_{Cl}$	$\chi^2_{red} = 375$ $E_0 = 5.2(6)$
Solution #3: 0.010 m $PdCl_2$ + 0.010 m HCl				
$2 \leqslant k \leqslant 12$ $1 \leqslant R \leqslant 5$	30 °C, 800 bar	$n_O = 1.3(3)$ $r_O = 2.04(2)$ Å σ^2_O§ $= 0.0009(5)$ Å^2	$n_{Cl} = 2.7(3)$ $r_{Cl} = 2.288(7)$ Å $\sigma^2_{Cl} = 0.0009(5)$ Å^2	$\chi^2_{red} = 295$ $E_0 = 8(1)$
$2 \leqslant k \leqslant 12$ $1 \leqslant R \leqslant 5$	70 °C, 800 bar	$n_O = 1.7(3)$ $r_O = 2.06(7)$ Å σ^2_O§ $= 0.0010(6)$ Å^2	$n_{Cl} = 2.3(3)$ $r_{Cl} = 2.298(7)$ Å $\sigma^2_{Cl} = 0.0010(6)$ Å^2	
$2 \leqslant k \leqslant 10$ $1 \leqslant R \leqslant 5$	97 °C, 800 bar	$n_O = 1.7(3)$ $r_O = 2.07(8)$ Å σ^2_O§ $= 0.0021(8)$ Å^2 $r_{Pd–O–Pd–O–Pd} = 2 \times rO$ $\sigma^2_{O\ Pd–O–Pd–O–Pd} = \sigma^2_O$	$n_{Cl} = 2.3(3)$ $r_{Cl} = 2.302(9)$ Å $\sigma^2_{Cl} = 0.0021(8)$ Å^2 $r_{Pd–Cl–Pd–Cl–Pd} = 2 \times rCl$ $\sigma^2_{Cl\ Pd–Cl–Pd–Cl–Pd} = \sigma^2_{Cl}$ $r_{Pd–Cl–Cl–Pd} = 2 \times rCl$ $\sigma^2_{Cl\ Pd–Cl–Cl–Pd} = \sigma^2_{Cl}$	

For all solutions, the concentration of Cl ≫ Pd.
* Attempts to refine n_O and n_{Cl} (with the constraint that the maximum $n_{Cl} = 2$, as determined from the composition of the solution) resulted in $n_O = n_{Cl} = 2$.
§ σ_O were constrained to be the same as σ_{Cl}.

The EXAFS data were analyzed with the HORAE package (Ravel and Newville, 2005) with FEFF version 9 (Rehr et al., 2010). The k^n-weighted data ($n = 1, 2, 3$) used in the fit ranged from 2.0 to 10–12 Å^{-1} ($T > 100$ °C and $T \leqslant 100$ °C, respectively). The fitting was done in R-space over the range 1.0–5 Å. EXAFS transmission signals were noisy and thus fluorescence data were used for the analyses. In addition, we performed *ab initio* XANES calculations for the K_2PdCl_4(s) standard (crystal structure from Hester et al., 1993), and for the square planar $[PdCl_4]$ and $[PdCl_2O_2]$ (cis- and trans-geometries) moieties. The photoabsorption cross-sections were calculated using the FDMNES package (Joly, 2001), following the procedure outlined in our earlier studies (e.g., Etschmann et al., 2010; Liu et al., 2011; Tooth et al., 2013). Calculations were made in 'Green' mode, with potential described using the muffin-tin approximation. To make the calculated raw cross-sections comparable with the experimental spectra, the raw calculations were convoluted with a Lorentzian function that has an energy-dependent width in order to reproduce the core–hole lifetime broadening (7.94 eV from the FDMNES database) and the inelastic plasmon interactions with the photoelectron, and with a Gaussian function to reproduce the experimental resolution, 1.22 eV in this case (Proux et al., 2005a,b).

A number of attempts were made to measure Pd–$S_{(aq)}$ complexes: (i) four repeat runs to 350 °C starting with $PdS_{(s)}$ in 2 m NaHS solution; and (ii) one run with Pd metal + $PdS_{(s)}$ in 2 m NaHS solution and 0.5 m NaBr. None of the runs resulted in trustworthy results. The repeat runs all showed different results, with two runs showing Pd near the detection limit (possibly from scattering of the PdS(s), as room-temperature runs in a large cell where the solid is further away from the beam showed no Pd edge, i.e. Pd ≪ 100 ppm). Useable XANES and EXAFS spectra were obtained from the other two runs, remarkably even at room temperate where the expected solubility is well below the detection limit of 100 ppm (based on

UNCORRECTED PROOF

Please cite this article in press as: Mei Y., et al. Palladium complexation in chloride- and bisulfide-rich fluids: Insights from *ab initio* molecular dynamics simulations and X-ray absorption spectroscopy. *Geochim. Cosmochim. Acta* (2015), http://dx.doi.org/10.1016/j.gca.2015.04.009

transmission step height). Furthermore, the XAS spectra were remarkably similar for *all* measured temperatures (in *E*, *k* and *R*-space), whereas previous solution experiments demonstrated that even if the geometry of the complex does not change, there is a significant decrease and widening of the dominant peak in *R*-space with increasing temperature (e.g., Tooth et al., 2011), suggesting that a solid was being measured in out runs. In the NaBr–NaHS run, $PdS_{(s)}$ solubility was below detection limit up to 70 °C. We note that the predicted Pd solubilities in HS-rich fluid are well below the detection limit (see Section 4).

2.4. Thermodynamic modeling

The plots were generated using the Geochemist's Workbench software (Bethke, 2008). Thermodynamic properties for the solid phases $Pd_{(s)}$ and $PdS_{(s)}$ were taken from Sassani and Shock (1998), and properties for Pd(II) chloride and bisulfide complexes are from the sources indicated on each figure. The other properties were from the Lawrence Livermore database (LLNL R9), as distributed with the Geochemist's Workbench.

3. RESULTS

3.1. Complex geometry via *ab initio* molecular dynamics simulations and comparison with XAS measurements

Ab initio MD simulations of Pd(II)–Cl complexes were performed at 125 °C, 14 bar (P_{sat}) and 300 °C, 500 bar. The resulting Pd–Cl and Pd–O bond distances and Debye–Waller factors are listed in Table 2. At 125 °C, simulation 1a was started with the octahedral Pd(II)–aqua complex, in order to test for the stability of this configuration. This confirmed the high stability of the square planar configuration, as two water molecules dissociated within 0.2 ps to form square planar $Pd(H_2O)_4^{2+}$ (Fig. 1a), which remained stable for the remaining more than 7 ps of simulation, with an average Pd–O distance of 2.07 Å and a Debye–Waller factor of 0.004 $Å^2$. When starting with the $PdCl(H_2O)_3^+$ structure (simulation 1b), the complex retained one chloride and three waters and kept the square planar $PdCl(H_2O)_3^+$ configuration over the length of the simulation (Fig. 1b). This simulation gave a Pd–Cl distance of 2.37 Å and a Debye–Waller factor of 0.005 $Å^2$; the three O in $PdCl(H_2O)_3^+$ show significantly different Pd–O distances. As shown in Fig. 1b, the O located at the trans-position relative to Cl (O_3) had a Pd–O distance of 2.12 Å, while the other two O that were in the cis-position compared to the Cl (O_1 and O_2) had shorter Pd–O distances at 2.07–2.08 Å, similar as observed in previous *ab initio* calculations (Pd–O distances of 2.080, 2.080, 2.155 Å by Boily and Seward, 2005).

Two different structures were observed for the $PdCl_2(H_2O)_2$(aq) complex depending on the initial configuration. Simulation 1c started with the cis-structure (Cl–Pd–Cl angle of 90°); the final structure was square planar cis-$PdCl_2(H_2O)_2$(aq) (Fig. 1c) with Pd–Cl distances of 2.37–2.38 Å and Pd–O distances of 2.11–2.12 Å (Table 2). When starting with the trans-structure, the Cl–Pd–Cl angle equilibrated at ~168° during the simulation (Fig. 1d) with Pd–Cl distances of 2.40 Å and Pd–O distances of 2.08 Å (Table 2). The simulation (1d) of the $PdCl_3(H_2O)^-$ complex was started with a square planar structure, which remained

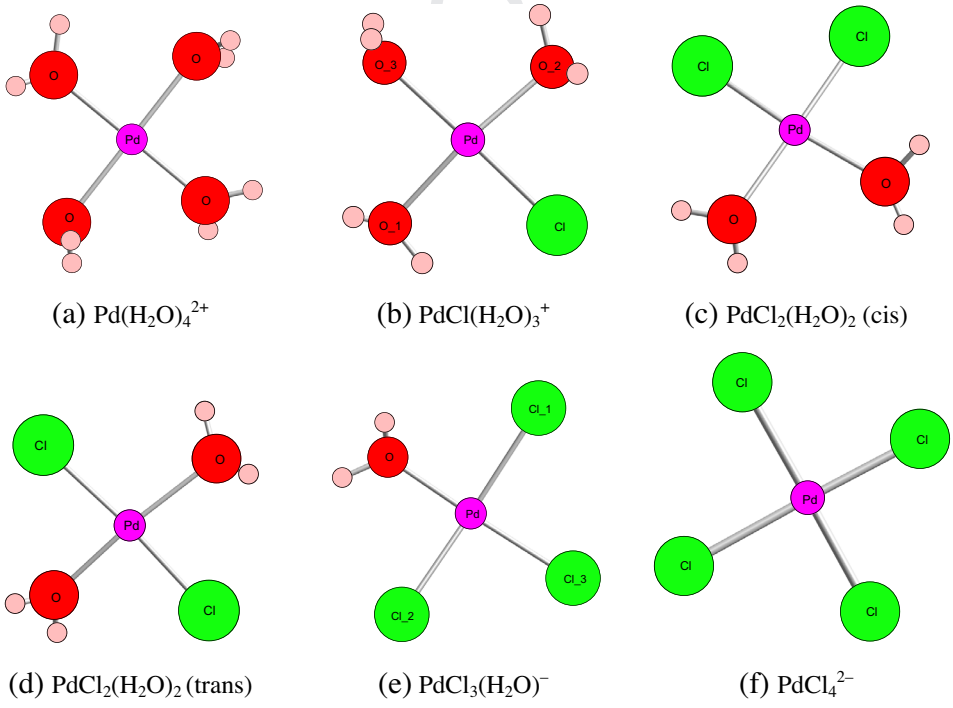

(a) $Pd(H_2O)_4^{2+}$ (b) $PdCl(H_2O)_3^+$ (c) $PdCl_2(H_2O)_2$ (cis)

(d) $PdCl_2(H_2O)_2$ (trans) (e) $PdCl_3(H_2O)^-$ (f) $PdCl_4^{2-}$

Fig. 1. Geometries of Pd(II)–Cl complexes.

stable during the whole simulation period (10 ps). The Pd–O distance in the $PdCl_3(H_2O)^-$ complex was 2.12 Å with the Debye–Waller factor of 0.006 $Å^2$, while Pd–Cl distances showed a significant spread: the Cl at the trans-position relative to O (Cl_3 in Fig. 1e) was located at a Pd–Cl distance of 2.38 Å, while the other two Cl at cis-position relative to O (Cl_1 and Cl_2 in Fig. 1e) had longer Pd–Cl distances at 2.40–2.41 Å. Simulation 1f was started with the square planar $PdCl_4^{2-}$ configuration, and this structure was stable over the 10 ps of the simulation, with Pd–Cl distances of 2.41–2.42 Å and Debye–Waller factors of 0.007–0.008 $Å^2$ (Fig. 1f).

Ab initio MD simulations gave similar geometry and speciation of Pd–Cl complexes at 300 °C, 500 bar. Simulations No. 2a,c,d,e were started with square planar $PdCl(H_2O)_3^+$, $PdCl_2(H_2O)_2$(trans), $PdCl_3(H_2O)^-$ and $PdCl_4^{2-}$ configurations, and all retained the initial square planar structure during the entire simulation period (more than 7 ps). To test the stability of tetrahedral structures, simulation 2b was started with the tetrahedral $PdCl_2(H_2O)_2$(aq). The tetrahedral structure broke within in 1 ps into the cis-square planar $PdCl_2(H_2O)_2$(aq) (Fig. 1c); this complex remained stable for the remaining simulation time (7 ps). The Pd–O and Pd–Cl bond distances are similar at 125 °C and 300 °C, while the Debye–Waller factors at 300 °C are slightly larger than at 125 °C (Table 2).

Experimental XAS data were collected to benchmark the MD calculations. The XANES part of the spectrum, which can be related to the geometry of the complexes, was examined first. The XANES spectra of the three Pd solutions are similar (Fig. 2a), with subtle variations that are a function of ligand and temperature. When Pd is bonded to four Cl ligands (solution S1), there are two peaks in the region between 24.35 and 24.40 keV (indicated by arrows), whereas where Pd is bonded to two O and two Cl ligands (solution S3), this part of the XANES spectrum shows a single broad peak (as shown by arrow). *Ab initio* calculations confirm that these experimental differences are consistent with a change from square planar $PdCl_4^{2-}$ to square planar $Pd(H_2O)_2Cl_2$(aq) (Fig. 2a). In addition, the calculations confirm that the extra band in the 24.35–24.40 keV region in the solid K_2PdCl_4(s) compared to solution S3, both of which contain the $[PdCl_4]$ moiety, is due to second shell effects (calculation with a 3 Å radius takes only the $[PdCl_4]$ moiety into account). In both S1 and S3, the height of the peaks in the 24.35–24.40 keV region increases with increasing temperature, indicative a subtle changes in complex geometry and structure of the second shell.

The *k*-space EXAFS and *R*-space Fourier transformed data are shown in Fig. 2b and c, including the multiple scattering paths used in the fits. The EXAFS results demonstrated that the Pd(II) complexes were always 4-coordinated (30–130 °C), in accordance with the MD results. The experimental Pd–Cl distances ranged from 2.274(5) to 2.305(2) Å and the Pd–O distances ranged from 2.022(9) to 2.07(8) Å depending on ligands and temperature (Fig. 2; Table 4). The Pd–Cl and Pd–O distances predicted by *ab initio* MD increased slightly with the increase of Cl in the first coordination shell as well as increasing temperature. For the $Pd(H_2O)_4^{2+}$ complex, *ab initio* MD simulations gave overall Pd–O distances of 2.07–2.08 Å, similar to the CPMD study of Beret et al. (2008a,b (2.06 Å). These distance are slightly longer than those obtained from the XAS measurements from this (2.02–2.07 Å, Table 3) and previous experiments (2.00–2.01 Å, Seward et al., 2002; Seward and Driesner, 2004; 2.01–2.04 Å, Boily and Seward, 2005; 2.00–2.04 Å, Bowron et al., 2011; 2.00–2.02 Å, Bazarkina et al., 2014). Such slightly longer bond distances in theoretical studies are inline with the expected accuracy of the DFT approach (e.g., Bühl et al., 2006). The increasing Pd–O distances in complexes with chlorides (2.07–2.14 Å) are in line with the static DFT study of Boily and Seward (2005) (2.04–2.13 Å) and experimental

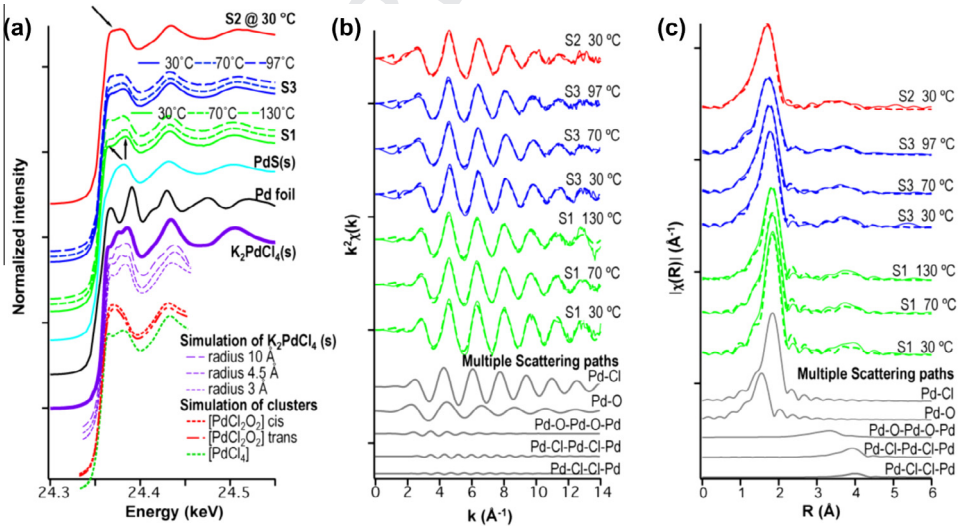

Fig. 2. XAS data for the three $PdCl_2$ solutions (composition as described in Table 4). (a) The XANES spectra compared to solid standards and *ab initio* XANES calculations; (b) k^2 weighted EXAFS data and scattering paths used in the fit; and (c) the magnitude of the Fourier transform and scattering paths used in the fit. Data are displayed as solid lines, and fits are dotted lines in (b) and (c).

Please cite this article in press as: Mei Y., et al. Palladium complexation in chloride- and bisulfide-rich fluids: Insights from *ab initio* molecular dynamics simulations and X-ray absorption spectroscopy. *Geochim. Cosmochim. Acta* (2015), http://dx.doi.org/10.1016/j.gca.2015.04.009

measurement by Bazarkina et al. (2014) (2.06–2.10 Å). The Pd–Cl distances predicted in our *ab initio* MD simulations for $PdCl_4^{2-}$ at 150 °C are 2.41–2.42 Å, which are in good agreement with the DFT results of Boily and Seward (2005): 2.42 Å at the B3LYP level (Becke, 1993), and 2.36 Å at the MP2 level (second order Møller–Plesset theory, Head-Gordon et al., 1988). These distances are longer than the experimental Pd–Cl distances (2.26–2.28 Å, Seward et al. (2002); 2.28–2.315 Å, Boily and Seward (2005); 2.30–2.31, Bazarkina et al. (2014); 2.305(2) Å in our measurements, Table 4), though within error, as determined by the standard deviation of average distances. Although a higher level of theory (i.e., MP2) gives a better prediction of the geometry of Pd complexes, density functional theory methods such as B3LYP provide satisfactory predictions compared with experiments (absolute values within 10%). The experimental Pd–Cl distances decrease to ~2.27 Å for lower order chloride complexes (e.g., $PdCl_2$(aq)); this decrease is consistent with the *ab initio* MD results (Table 2). The thermal disorder (Debye–Waller factors) obtained from the simulations for Pd-Cl in $PdCl_4^{2-}$ increased from ~0.007 at 125 °C to 0.009 at 300 °C, which compares well with experimental values of 0.0010(3) (30 °C), 0.0027(3) (70 °C) and 0.0035(5) $Å^2$ (130 °C).

The results of the *ab initio* MD simulations for the Pd(II) complexes in HS-rich solutions are listed in Table 3. Simulation 3a was started with the initial configuration of octahedral $Pd(H_2O)_6^{2+}$, which broke quickly (0.2 ps) by releasing two water molecules to form a square planar $Pd(H_2O)_4^{2+}$ complex (same as in Fig. 1a). However, within 1 ps of simulation time, one water in $Pd(H_2O)_4^{2+}$ was deprotonated, forming $Pd(OH)(H_2O)_3^+$ (Fig. 3a) and HS^- associated with one H and formed H_2S(aq). After 7.2 ps, one more hydrogen was deprotonated, and the neutral species $Pd(OH)_2(H_2O)_2$(aq) (Fig. 3b) formed and remained stable for the remaining 3.6 ps of the simulation. In terms of pH, this evolution corresponds to a change of bulk solution pH from highly alkaline ($\gg pK_a(H_2S)$) to near $pK_a(H_2S)$. In $Pd(OH)(H_2O)_3^+$ and $Pd(OH)_2(H_2O)_2$, different "types" of O gave different Pd–O bond distances (Fig. 3a). In $Pd(OH)(H_2O)_3^+$, the O belonging to the OH^- group has the shortest Pd–O distance of 2.02 Å (O_1 in Fig. 3a). Among the O belonging to H_2O groups, the two O at 90° relative to OH^- gave Pd–O distances of 2.11–2.12 Å (O_2 and O_3), while the O at linear position relative to OH^- (O_4) gave the longest Pd–O distance of 2.16 Å. Similarly, in $Pd(OH)_2(H_2O)_2$(aq) the Pd–OH (O_1 and O_2 in Fig. 3b) bonds are shorter than the Pd–OH_2 bond (O_3 and O_4).

Simulation 3b was started with the tetrahedral $PdHS(H_2O)_3^+$ structure, changed quickly to square planar complex $PdHS(H_2O)_3^+$, and then remained stable for 8 ps (see Fig. 3c and Table 3 for geometrical parameters). The tetrahedral complex $Pd(HS)_2(H_2O)_2$(aq) in simulation 3c also changed to a square planar (cis) structure and remained stable for the rest of the simulation (Fig. 3d; Table 3). In simulation 3d, the initial configuration was the trans-square planar $Pd(HS)_2(H_2O)_2$(aq) structure, and remained as such for 5.3 ps (Fig. 3e) before deprotonation of a H_2O took place, resulting in the formation of $[Pd(HS)_2(OH)(H_2O)]^-$ (Fig. 3f). *Ab initio* MD simulations initiated with 3 and 4 HS^- ligands around Pd(II) also ended with square planar complexes (Fig. 3g, h; Table 3). The Pd–S distances in the $Pd(HS)_n^{2-n}$ complexes showed a slight increase from $n = 1$ to $n = 4$. The Debye–Waller factor of

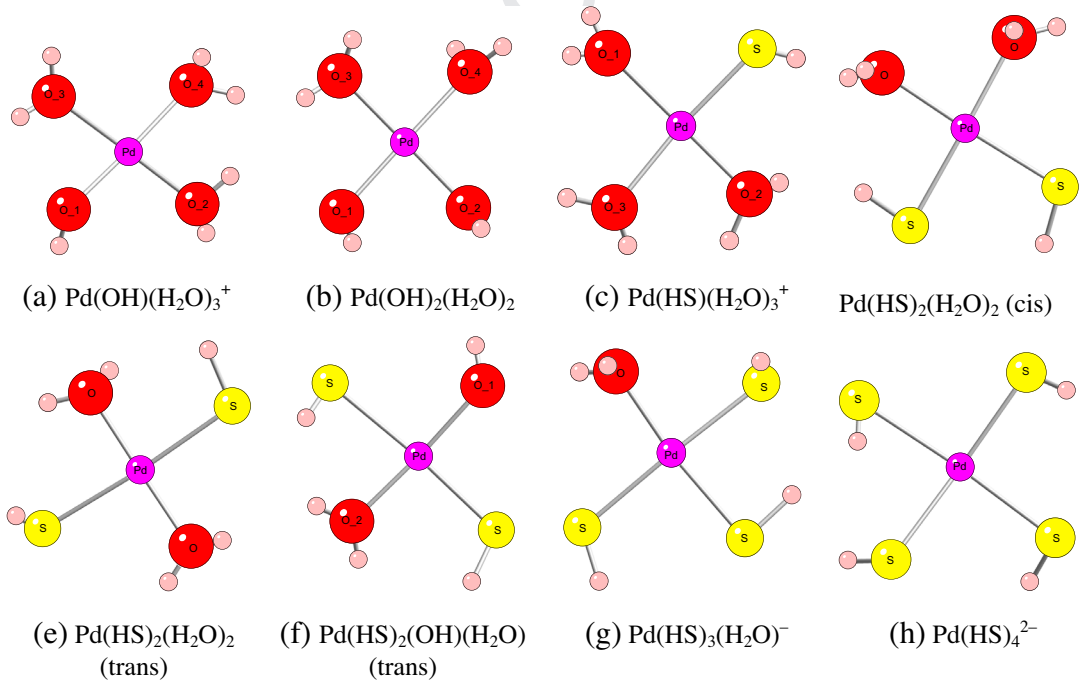

Fig. 3. Geometries of Pd(II)–HS complexes.

Please cite this article in press as: Mei Y., et al. Palladium complexation in chloride- and bisulfide-rich fluids: Insights from *ab initio* molecular dynamics simulations and X-ray absorption spectroscopy. *Geochim. Cosmochim. Acta* (2015), http://dx.doi.org/10.1016/j.gca.2015.04.009

Pd–OH is smaller than that of Pd–OH_2, indicating a decrease in the oscillation of Pd–O bond when Pd(II) is complexing with OH^- relative to H_2O. These subtle differences in bond distances and Debye–Waller factors indicate a stronger association between Pd–OH than Pd–OH_2.

3.2. *Ab initio* free energy calculations

The results of the *ab initio* MD simulations described above provide qualitative information about the geometrical properties of different Pd(II)–Cl and Pd(II)–HS complexes. However, all Pd(II) complexes listed in Figs. 1 and 3 are (meta-)stable during 5–10 ps, and therefore these calculations do not provide any information about the relative stabilities of these complexes, which is key to understanding Pd transport in Cl-HS-brines. As it is not practical to run *ab initio* MD at the time scale of ligand-exchange for these complexes (i.e., microseconds), we chose to apply distance-constrained thermodynamic integration to retrieve free energy information for the different ligand exchange reactions. The chosen approach is illustrated in Fig. 4 for the ligand exchange reaction:

$$PdCl(H_2O)_3^+ + H_2O = Pd(H_2O)_4^{2+} + Cl^- \quad (4)$$

The Helmholtz free energy $\Delta_r A_{a\to b}$ of reaction (4) was calculated by integrating the constraint mean force required to shift the coordinated Cl atom from its equilibrium position to a non-interacting position. As shown in Fig. 4, the force is close to zero (5.22 kJ $Å^{-1}$ mol^{-1}) at 2.35 Å – the distance corresponding to the equilibrated Pd–Cl bond distance in the unconstrained *ab initio* MD simulations. With increasing Pd–Cl distance, an external force must be applied to maintain a given Pd–Cl distance because of the attraction between Pd and Cl. The maximum absolute value of the constraint force is reached at a distance of 2.8 Å (−126.48 kJ $Å^{-1}$ mol^{-1}); then the absolute magnitude of the force decreases with increasing Pd–Cl distance. The constraint force becomes zero again at a distance at 3.0–3.1 Å and at this stage Cl is dissociated from Pd and one water molecule complexed to Pd. As shown in Fig. 4, the maximum energy barrier of dissociation (defined as the activation energy of dissociation, E_{a_dis}) of +69.75 kJ mol^{-1} is reached for reaction (4) at 3.1 Å. The mean constraint forces become slightly positive in the range of 3.1–4.3 Å, which results from the outer solvation shell and reflects the activation barrier for the ion exchange reaction. Beyond the Pd–Cl distance of 4.5 Å, the force between Pd^{2+} and Cl^- is negligible. In contrast, the maximum energy barrier of association (E_{a_as}) from Pd^{2+} to $PdCl^+$ is 17.5 kJ mol^{-1}, as shown in Fig. 4. Integration of the mean constraint force along the reaction coordinates gives a free energy difference ($\Delta_r A_{PdCl^+\to Pd^{2+}}$) of +56.82 kJ mol^{-1} for reaction (4).

The energy surfaces for the dissociation reactions of the $PdCl_2(H_2O)_2$(aq), $PdCl_3(H_2O)^-$ and $PdCl_4^{2-}$ complexes were obtained using the same method, and are plotted in Fig. 5. For $PdCl_2(H_2O)_2$(aq) (reaction $PdCl_2(H_2O)_2(aq) + H_2O = PdCl(H_2O)_3^+ + Cl^-$; Fig. 5b), the E_{a_dis} is +51.88 kJ mol^{-1} at 3.0 Å, indicating that the Cl^- dissociated from Pd at this distance. The E_{a_dis} are 57.93 kJ mol^{-1} and 52.48 kJ mol^{-1} for $PdCl_3(H_2O)^-$ and $PdCl_4^{2-}$ stepwise dissociation reactions, respectively (Fig. 5c, d) at distances around 3.2 Å. Whereas similar E_{a_dis} (51–58 kJ mol^{-1}) were obtained for the $PdCl_n^{n-2}$ ($n = 2, 3, 4$) complexes, the E_{a_as} values show larger variations. The association reaction from $PdCl^+$ to $PdCl_2$(aq) has an activation energy E_{a_as} of 15.79 kJ mol^{-1} (Fig. 5b), while the E_{a_as} values of the stepwise association reactions for forming $PdCl_3(H_2O)^-$ from $PdCl_2$(aq) (Fig. 5c) and $PdCl_4^{2-}$ from $PdCl_3(H_2O)^-$ (Fig. 5d) are 25.03 kJ mol^{-1} and 34.76 kJ mol^{-1}, respectively. The larger E_{a_as} for forming $PdCl_3(H_2O)^-$ and $PdCl_4^{2-}$ correspond to smaller Helmholtz free energies for the Pd–Cl dissociation reactions.

Free energy surfaces of the Pd(II)–HS dissociation reactions were also calculated using the same method. In these

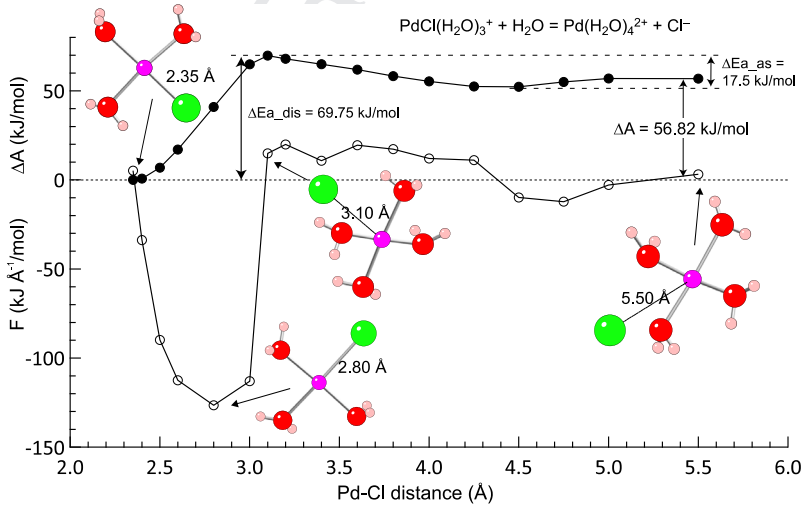

Fig. 4. Example of distance constraint thermodynamic integration for calculating the Free Energy of a ligand exchange reaction. F (empty cycle line) is the mean constraint force needed to keep Pd–Cl at certain distance, and ΔA (solid cycle line) is the integral of mean constraint force (F) with respect to the constrained distances calculated by Eq. (1).

Please cite this article in press as: Mei Y., et al. Palladium complexation in chloride- and bisulfide-rich fluids: Insights from *ab initio* molecular dynamics simulations and X-ray absorption spectroscopy. *Geochim. Cosmochim. Acta* (2015), http://dx.doi.org/10.1016/j.gca.2015.04.009

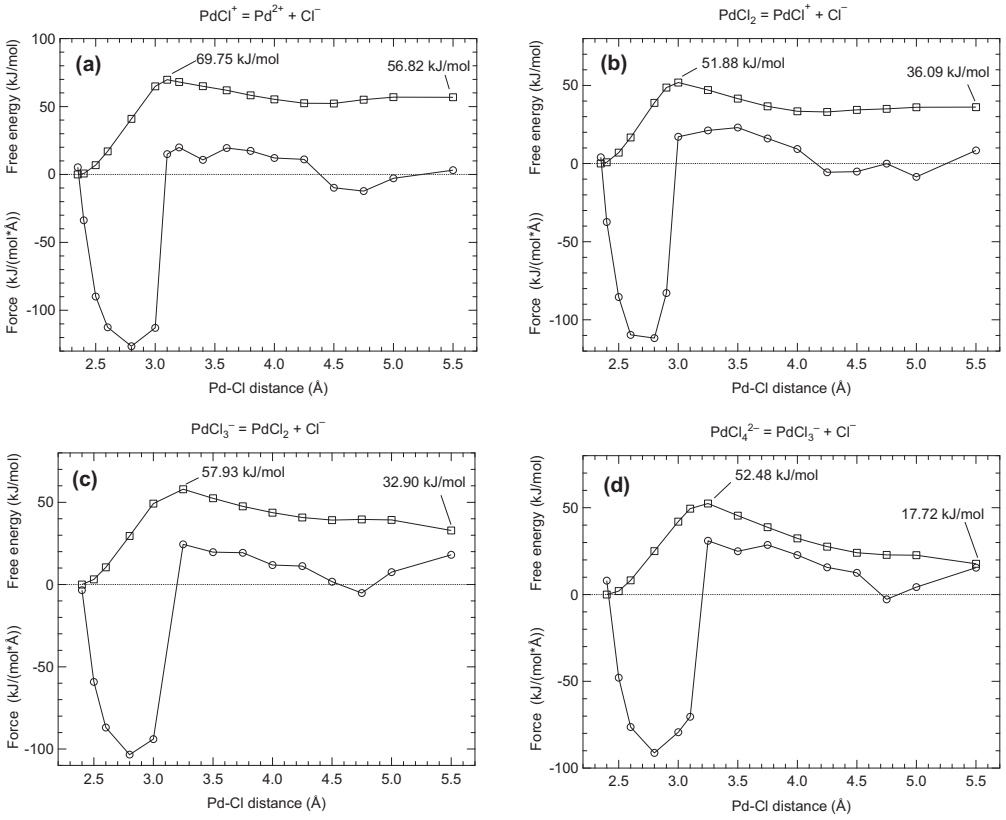

Fig. 5. Mean constrained force (cycles in lines) and free energy (squares in lines) of Pd–Cl dissociation reactions at 300 °C, 500 bar.

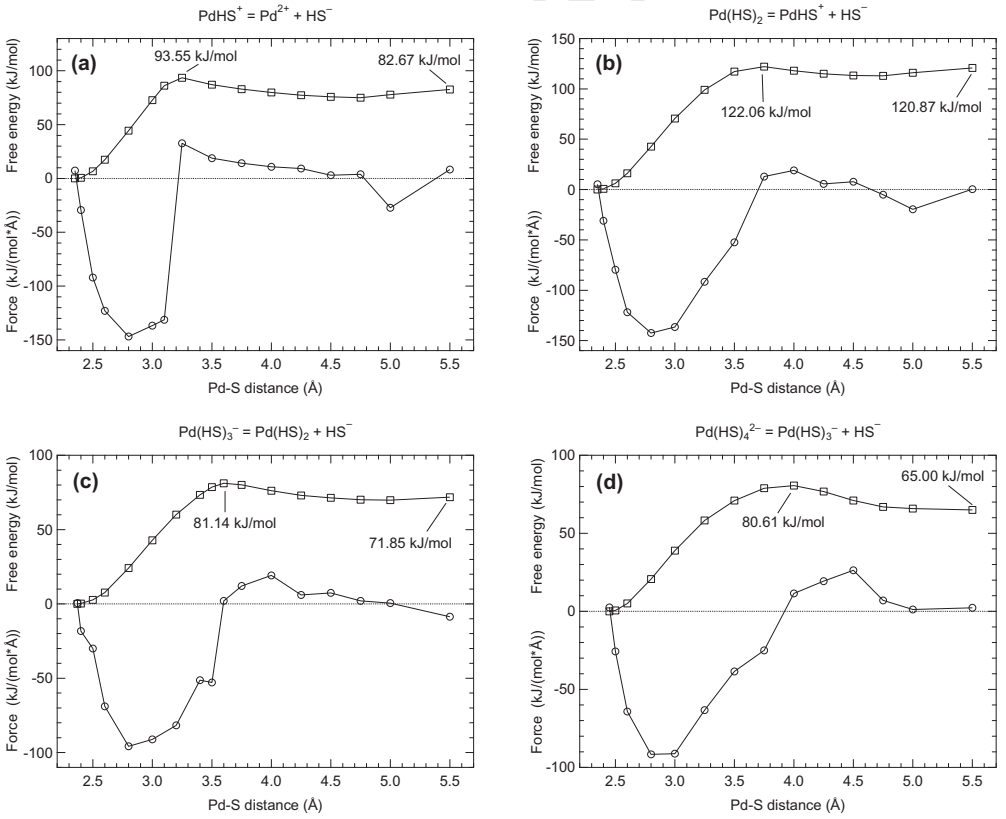

Fig. 6. Mean constrained force (cycles in lines) and free energy (squares in lines) of Pd–HS dissociation reactions at 300 °C, 500 bar.

Table 5a
Free energy and thermodynamic properties for the stepwise formation constants of Pd–Cl and Pd–HS complexes at 300 °C and 500 bar (data fitted from HKF parameters provided in Tagirov et al., 2013).

Reaction	$\Delta_r G(P, T)$ (kJ mol^{-1})	$\Delta_r G^{\Theta,c}(P, T)$ (kJ mol^{-1})	$\Delta_r G^{\Theta}(P_r, T_r)$ (kJ mol^{-1})	$\log K^{\Theta}$ (P, T)	$\log K$ Tagirov et al. (2013)
$Pd^{2+} + Cl^- = PdCl^+$	−56.817	−46.098	−66.707	6.08	5.11
$PdCl^+ + Cl^- = PdCl_2(aq)$	−36.093	−26.993	−36.995	3.37	4.12
$PdCl_2 + Cl^- = PdCl_3^-$	−32.899	−26.293	−27.045	2.46	2.75
$PdCl_3^- + Cl^- = PdCl_4^{2-}$	−17.724	−17.724	−8.699	0.79	0.70*
$Pd^{2+} + HS^- = Pd(HS)^+$	−82.665	−71.946	−92.555	8.43	–
$PdHS^+ + HS^- = Pd(HS)_2(aq)$	−120.873	−111.773	−121.775	11.1	–
$Pd(HS)_2 + HS^- = Pd(HS)_3^-$	−71.848	−65.242	−65.994	6.01	2.50
$Pd(HS)_3^- + HS^- = Pd(HS)_4^{2-}$	−64.997	−64.997	−55.972	5.10	–

* The value obtained by Bazarkina et al. (2014) at 300 °C, 600 bar is 0.4(1).

calculations, Pd–S distances were constrained in step-wise dissociation/association reactions and the mean forces to maintain the distance were recorded. The forces and their integrals (free energy) are shown in Fig. 6. Overall the dissociation energies of the Pd–HS complexes are very positive, which reflects the strong tendency of Pd(II) to react with HS^- to form $Pd(HS)_n^{n-2}$ ($n = 1$–4). The free energy of dissociation of $PdHS^+$ is 82.67 kJ mol^{-1} with the E_{a_dis} of 93.55 kJ mol^{-1} at 3.25 Å, indicating that the dissociation of $Pd(HS)^+$ happened at distance around 3.2 Å. Conversely, the stepwise dissociation of $Pd(HS)_2(aq)$ happens at longer distances around 3.75 Å (Fig. 6b) with the E_{a_dis} of 122.06 kJ mol^{-1}, which is higher than the E_{a_dis} of $Pd(HS)^+$. The high activation energy of dissociation of $Pd(HS)_2(aq)$ indicates that more energy is needed to dissociate one HS^- ligand in $Pd(HS)_2(aq)$ than in $Pd(HS)^+$ complex. The stepwise dissociations of $Pd(HS)_3^-$ and $Pd(HS)_4^{2-}$ happen at distances around 3.6 Å and 4.0 Å, with an E_{a_dis} of 81.14 kJ mol^{-1} and 80.61 kJ mol^{-1}, respectively (Fig. 6c, d).

The free energy calculations (Figs. 5 and 6) demonstrate that the dissociation of Pd(II)–HS complexes happens at longer Pd–S distances (3.2–4.0 Å) compared with Pd(II)–Cl complexes (3.1–3.2 Å), resulting in a larger $\Delta_r A$ and in larger E_{a_dis} of Pd–HS dissociation. The stepwise stability constants ($\log K$) and cumulative formation constants ($\log \beta$) of different Pd–Cl and Pd–HS complexes were calculated after concentration and activity corrections (Mei et al., 2013a, 2015), and are listed in Table 5 together with the values derived from experimental studies by Tagirov et al. (2013) and Wood et al. (1992).

4. DISCUSSION

4.1. Nature of Pd(II)–Cl and Pd(II)–HS complexes

Knowledge of the coordination geometry of aqueous complexes allows constraints to be placed on the number and nature of possible species (e.g., Etschmann et al., 2011). Numerous Pd(II) complexes display a square planar geometry (Mason and Gray, 1968; Vanquickenborne and Ceulemans, 1981), and our *ab initio* MD simulations confirm that the Pd(II) aqua ion as well as all Pd(II) chloride and bisulfide complexes share a square planar geometry. The square planar geometry is shared with Au(III) aqua, hydroxide and halide complexes (Usher et al., 2009; Liu et al., 2014), but makes Pd different from divalent first row transition metals (Mn(II), Fe(II), Co(II), Ni(II), Zn(II)), which display octahedral and tetrahedral geometries (e.g., Susak and Crerar, 1985; Hoffmann et al., 1999; Liu et al., 2011; Tian et al., 2013, 2014).

4.2. Comparison with previous studies

As shown in Table 5 and Fig. 7a, the cumulative formation constants ($\log \beta$) for Pd(II)–Cl complexes derived from the *ab initio* MD simulations are in good agreement with

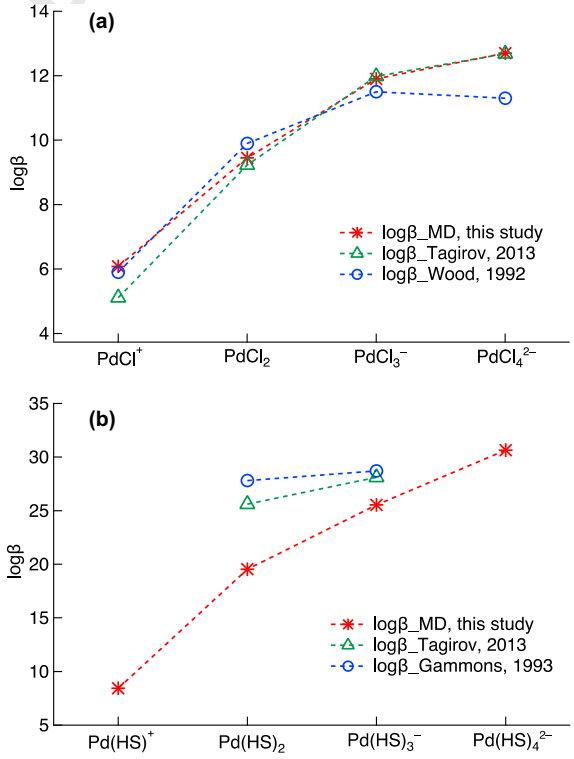

Fig. 7. Formation constants of Pd–Cl (a) and Pd–HS (b) complexes comparing with experiments at 300 °C, 500 bar, data of $\log \beta$ from Table 5b.

UNCORRECTED PROOF

Table 5b
Logarithm of cumulative formation constants of Pd–Cl and Pd–HS complexes at 300 °C, 500 bar (data fitted from HKF parameters provided in Tagirov et al., 2013) or 300 °C, P_{sat} (data in Wood et al., 1992; Gammons and Bloom, 1993; Pan and Wood, 1994).

Reaction	$\log\beta^{\Theta}(P, T)$				
	This study	Tagirov et al. (2013)	Pan and Wood (1994)	Wood et al. (1992)	Gammons and Bloom (1993)
$Pd^{2+} + Cl^- = PdCl^+$	6.08	5.11		5.9	
$Pd^{2+} + 2\ Cl^- = PdCl_2(aq)$	9.45	9.23		9.9	
$Pd^{2+} + 3\ Cl^- = PdCl_3^-$	11.9	12.0		11.5	
$Pd^{2+} + 4\ Cl^- = PdCl_4^{2-}$	12.7	12.7		11.3	
$Pd^{2+} + HS^- = Pd(HS)^+$	8.43	–			
$Pd^{++} + 2\ HS^- = Pd(HS)_2(aq)$	19.53	25.6	29.8		27.8
$Pd^{++} + 3\ HS^- = Pd(HS)_3^-$	25.54	28.1			28.7
$Pd^{++} + 4\ HS^- = Pd(HS)_4^{2-}$	30.64	–			

the experimental studies of Wood et al. (1992) and Tagirov et al. (2013). The MD derived $\log\beta$ values plot between the two experimentally derived values, and the $\log\beta$ values for the $PdCl_2(aq)$, $PdCl_3^-$ and $PdCl_4^{2-}$ complexes calculated by MD simulations are very close to the recent experimental results of Tagirov et al. (2013). The quality of the agreement and the capacity of *ab initio* MD to provide useful thermodynamic properties is emphasized by the fact that the differences between the *ab initio* MD properties and experimental results are smaller than the differences between the properties derived by the two experimental groups. Hence, our *ab initio* MD simulations confirm the high stability of the $PdCl_4^{2-}$ complex in chloride-rich fluids as demonstrated by Tagirov et al. (2013) and Bazarkina et al. (2014).

The agreement among MD simulations and previous experimental studies for the formation constants of Pd(II)–HS complexes is poorer compared to Pd(II)–Cl complexes (Fig. 7b); however, this is likely to reflect the difficulties in conducting experiments about these complexes rather than limitations with the MD method. The experimental studies (Gammons and Bloom, 1993; Tagirov et al., 2013) only provided properties for two species, $Pd(HS)_2(aq)$ and $Pd(HS)_3^-$, while MD simulations calculated the properties for $Pd(HS)_n^{n-2}$ ($n = 1$–4) at 300 °C. The formation constants of $Pd(HS)_2(aq)$ and $Pd(HS)_3^-$ calculated from *ab initio* MD are a few orders of magnitudes lower than the experimental determinations (Table 5b, Fig. 7b). However, *ab initio* MD simulations suggest the high stability of the $Pd(HS)_4^{2-}$ complex ($\log\beta$ of 30.64 at 300 °C and 500 bar). This species, which is analogous to the highly stable $PdCl_4^{2-}$ complex, had not been taken in consideration by previous authors in the interpretation of experimental studies.

The $\log\beta$ values calculated from *ab initio* MD reveal that Pd(II)–HS complexing is stronger than Pd(II)–Cl. The

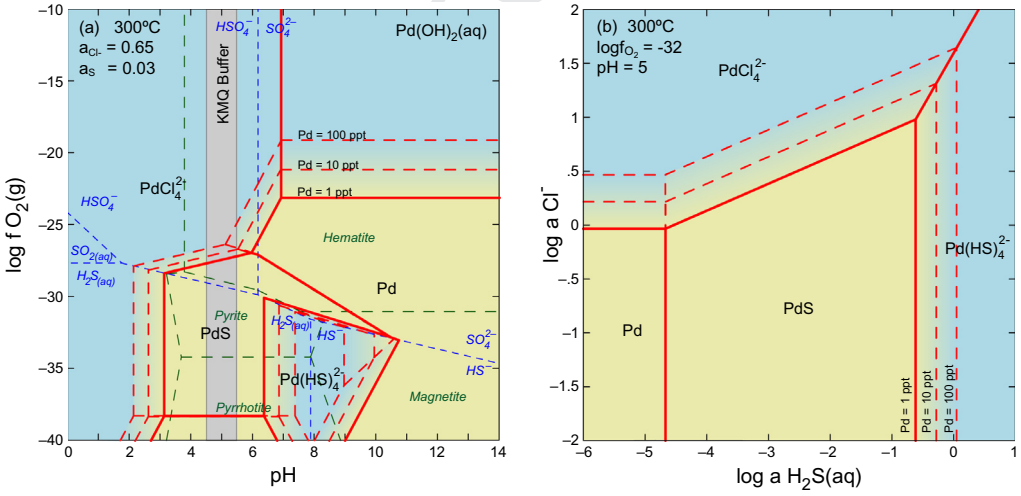

Fig. 8. Solubility and speciation of Pd at 300 °C, calculated with the properties of Pd(II) chloride and bisulfide complexes derived from *ab initio* principles in this study. (a) pH-Eh activity diagram for the predominant Pd species at 300 °C, 500 bar. Activities of 0.65 and 0.03 are chosen for Cl^- and S species, respectively, which represent 3 m of [Cl] and 0.12 m of [S] ($\gamma_{Cl^-} = 0.21$; $\gamma_{HS^-} = 0.25$). The dash blue lines show the boundary of different sulfur species; the dash green lines show the field of minerals as redox buffer, the gray bar shows the KMQ (K-feldspar–muscovite–quartz) buffer ($a_{K+} = 0.1$–0.01). (b) Comparison of mineral solubility and predominant aqueous Pd(II) species in Cl^- and H_2S rich fluids at 300 °C, 500 bar. pH of 5 and $\log f O_2$(g) of −34 is chosen to represent near neutral and moderate oxidation state conditions. (For interpretation of the references to color in this figure legend, the reader is referred to the web version of this article.)

Please cite this article in press as: Mei Y., et al. Palladium complexation in chloride- and bisulfide-rich fluids: Insights from *ab initio* molecular dynamics simulations and X-ray absorption spectroscopy. *Geochim. Cosmochim. Acta* (2015), http://dx.doi.org/10.1016/j.gca.2015.04.009

stronger complexing of bisulfide with Pd(II) is also shown in the free energy profile (Fig. 6) compared with Pd(II)–Cl (Fig. 5). As described in Section 3.3, the dissociation of Pd–Cl happened at a Pd–Cl distance of 3.25 Å, while for Pd–HS complexes the dissociation of Pd–S happened at longer distances of up to 3.75 Å.

4.3. Relative importance of Pd(II)–Cl and Pd(II)–HS species

Using the stability constants of Pd(II)–Cl and Pd(II)–HS complexes calculated by *ab initio* MD simulations, we constructed a diagram that shows the predicted mineral solubility and complex predominance as function of pH and fugacity of $O_2(g)$ in solutions containing 1–100 ppt of Pd^{2+}. The Cl^- activity of 0.65 and activity of predominant S species of 0.03 were chosen corresponding to the fluids with ~3 molal of Cl_{tot} and 0.12 molal of S_{tot} ($\gamma_{Cl^-} = 0.21$; $\gamma_{HS^-} = 0.25$) at 300 °C, 500 bar (Fig. 8a). Under oxidized conditions (sulfate stable), the chloride complex $PdCl_4^{2-}$ predominates in a 3 molal Cl_{tot} solution at acidic conditions. In contrast, under more reduced conditions near pyrite/pyrrhotite boundary and at pH values near the pK_a of $H_2S_{(aq)}/HS^-$, the bisulfide complex $Pd(HS)_4^{2-}$ predominates. The change of predominant species as the function of Cl^- and HS^- activity is plotted in Fig. 8b, which demonstrates that $PdCl_4^{2-}$ and $Pd(HS)_4^{2-}$ are the predominant species in Cl^- and bisulfide rich fluids, respectively.

4.4. Pd solubility as a function of pH and oxidation state

We further investigated the effect of pH and oxygen fugacity on Pd solubility and speciation in a simple hydrothermal solution containing 3 molal Cl_{tot}, 0.12 molal S_{tot} and Na^+ to balance the charge. Firstly, we calculated the effect of oxygen fugacity in Pd solubility and related speciation. In this calculation, the $pH_{300\ °C}$ was fixed to 5 to reproduce the slightly acidic conditions of hydrothermal fluids at the KMQ (K-feldspar–muscovite–quartz) pH buffer (see Fig. 8a). The Pd minerals controlling Pd solubility in the simulation are PdS(s) and Pd(s) when $\log fO_{2(g)}$ is −40 to −27, and Pd(s) at higher $\log fO_{2(g)}$ (Fig. 9a). Palladium solubility is ~0.01 ppb under reducing condition ($fH_{2(g)} > 1$; $\log fO_{2(g)} = < -38$). With increasing fugacity of $O_{2(g)}$, the total concentration of Pd drops more than three orders of magnitude to reach a minimum near the $H_2S(aq)/HSO_4^-$ coexistence line. A further increase in $fO_{2(g)}$ dramatically increases Pd solubility due to the contribution of Pd–Cl complexes. The abrupt change in solubility between the oxidation state of $\log fO_{2(g)} = -30$ to −26 is associated with a change of Pd mineral association from $PdS_{(s)}$ + native Pd to native Pd only (i.e., $PdS_{(s)} + 1.5\ O_{2(g)} + H_2O_{(l)} = Pd_{(s)} + HSO_4^- + H^+$).

To investigate the effect of pH on Pd speciation, we calculated mineral solubility in a solution containing 3 molal of chloride and 0.12 molal of sulfur at moderate redox condition ($\log fO_{2(g)} = -34$, near pyrite/pyrrhotite boundary at 300 °C). As shown in Fig. 9b, $PdCl_4^{2-}$ is the most abundant species when pH < 4, with concentrations 2 orders of magnitude higher than those of $PdCl_3^-$. With increasing pH, the bisulfide complex $Pd(HS)_4^{2-}$ became more important and overtook $PdCl_4^{2-}$ at $pH_{300\ °C} = 4$. $Pd(HS)_4^{2-}$ remained the predominant hydrosulfide species up to highly basic pH.

4.5. Geochemical implication

Palladium transport in oxidized chloride brines can now be modeled with a high degree of certainty, because the thermodynamic properties for Pd(II) chloride complexes based on our MD study are in excellent agreement with the recent experimental study by Tagirov et al. (2013). There is much evidence of Pd mobility under such conditions (i.e., hematite stable), e.g., in the Au–Pd province of the Minas Gerais, Brazil (Cabral et al., 2003, 2009).

In contrast, predictions of Pd mobility in bisulfide-rich fluids are highly dependent upon the chosen model. In a recent study, Barnes and Liu (2012) used thermodynamic modeling to explain observed Pd and Pt distribution in komatiite and related sulfur-rich rocks and ores. Their

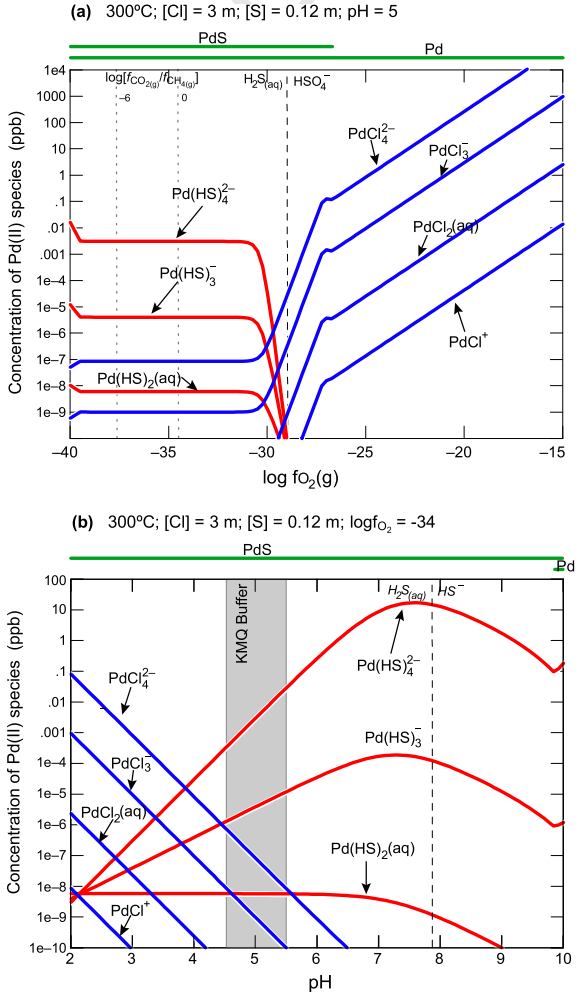

Fig. 9. Pd Speciation plot as a function of (a) $fO_2(g)$ and (b) pH based on the association constants for Pd(II) chloride and bisulfide complexes calculated from MD simulations in this study. (a: $S_{tot} = 0.12$ molal, $Cl_{tot} = 3$ molal, pH = 5; b: $S_{tot} = 0.12$ molal, $Cl_{tot} = 3$ molal, $\log fO_2(g) = -34$, near pyrite/pyrrhotite boundary).

Please cite this article in press as: Mei Y., et al. Palladium complexation in chloride- and bisulfide-rich fluids: Insights from *ab initio* molecular dynamics simulations and X-ray absorption spectroscopy. *Geochim. Cosmochim. Acta* (2015), http://dx.doi.org/10.1016/j.gca.2015.04.009

modeling based on the available experimental data on Pt and Pd solubilities (e.g., Wood et al., 1992; Gammons and Bloom, 1993; Pan and Wood, 1994) suggests that high mobility of Pd in S-rich rock and ores is due to high Pd solubilities as hydrosulfide complexes in acidic–neutral solutions under reduced and moderate oxidation conditions. In view of the new experimental data on Pd solubility by Tagirov et al. (2013) and our MD results, it is necessary to re-estimate Pd mobility in hydrothermal systems such as this case. We calculated Pd solubility and speciation as a function of pH and oxidation state in a hydrothermal fluid based on three thermodynamic data sources for Pd(II) chloro- and bisulfide-species (Wood et al., 1992; Gammons and Bloom, 1993; Tagirov et al., 2013); and *ab initio* MD-based properties from this study) are plotted in Fig. 10a and b.

As shown in Fig. 10a, under reduced conditions where Pd–bisulfide species predominate, the Pd solubility calculated using the *ab initio* MD-based $\log\beta$ for Pd species are about 3 orders of magnitude lower than those based on Wood et al. (1992) and Gammons and Bloom (1993), but close to the Pd solubility based on Tagirov et al. (2013); in contrast, in fluids with low total sulfur activity where the chloride complexes predominate, *ab initio* MD predicts the same solubility as using Tagirov et al.'s (2013) results, but higher solubilities than using Wood et al.'s (1992) properties. Fig. 10b further demonstrates that in reduced fluids (pyrite/pyrrhotite stable), Pd solubility reaches a maximum of several ppb at $pH_{300\,^\circ C} \approx 7$–8, indicating that Pd can be transported as bisulfide complexes under fluid-buffered conditions (e.g., HS^-/H_2S(aq) pH buffer) rather than rock-buffered conditions (e.g., quartz–feldspar–muscovite pH buffer). In summary, our study confirms that Pd is mainly carried by hydrosulfide as $Pd(HS)_4^{2-}$ at neutral-alkaline and reduced (pyrite/pyrrhotite stable) conditions and by chloride as $PdCl_4^{2-}$ at acidic and oxidized conditions.

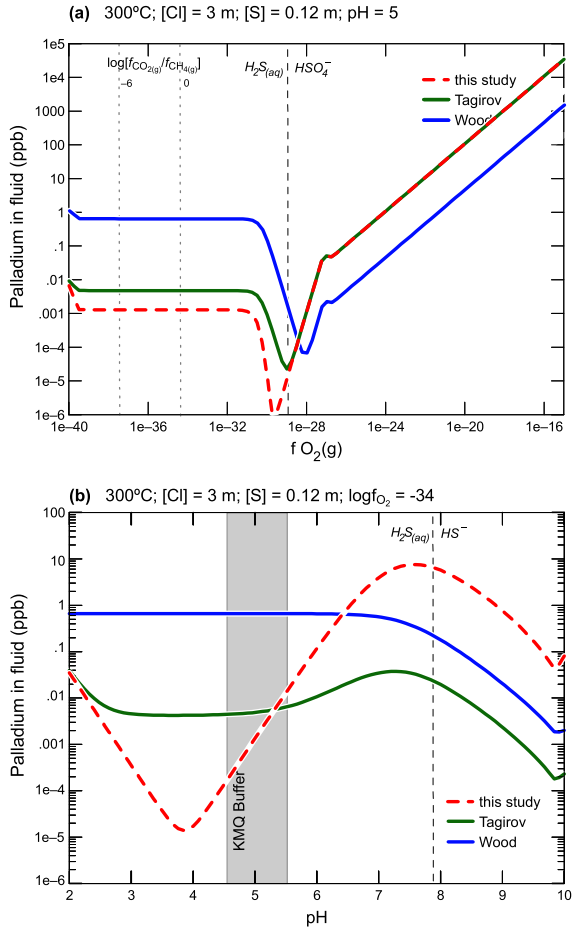

Fig. 10. Solubility of Pd as a function of fO_2(g) (a) and pH (b) in solution contains 0.12 molal S_{tot}, 3 molal Cl_{tot} and $\log fO_2(g) = 34$ (near pyrite/pyrrhotite boundary). Three different sets of $\log\beta$ are employed to compare the $\log\beta$ from this study with experimental values (Wood et al., 1992; Gammons and Bloom, 1993; Tagirov et al., 2013; $\log\beta$ listed in Table 5b).

5. CONCLUSION

This study illustrates the coming of age of quantitative *ab initio* MD methods for the exploration of metal complexation under hydrothermal conditions. The mineral solubilities predicted using experimentally derived properties and the theoretical values are in very good agreement, and the MD based properties can be used to make useful predictions of metal transport and deposition under hydrothermal conditions. Where significant discrepancies exist, the *ab initio* MD results provide a guide to prioritize additional experimental work and/or reinterpret existing experimental data (see also Mei et al., 2015).

UNCITED REFERENCE

Sherman (2007). Q7

ACKNOWLEDGEMENTS

We acknowledge the financial support of the Australian Research Council (ARC) through grant LP120100668 and DP130100471, and of the Minerals and Energy Research Institute of Western Australia (MERIWA) through grant M413. The authors thank the ESRF-CRG for the beamtime, and Australian International Synchrotron Access Program (ISAP) for travel funding. The MD calculations were supported by Pawsey Supercomputing Centre through the use of advanced computing resources located in Perth, Australia. M.L.F acknowledges the ARC as a recipient of an ARC Future Fellowship (FT110100241). This is contribution 592 from the ARC Centre of Excellence for Core to Crust Fluid Systems (http://www.ccfs.mq.edu.au). We are grateful to Dr. Artas Migdisov and two anonymous reviewers for their helpful comments on this manuscript. Q8 Q9

REFERENCES

Barnes S. J. (2004) Komatiites and nickel sulfide ores of the Black Swan area, Yilgarn Craton, Western Australia. 4. Platinum group element distribution in the ores, and genetic implications. *Miner. Deposita* **39**, 752–765.

Barnes S. J. and Liu W. (2012) Pt and Pd mobility in hydrothermal fluids: evidence from komatiites and from thermodynamic modelling. *Ore Geol. Rev.* **44**, 49–58.

UNCORRECTED PROOF

Barnes S. J., Heggie G. J. and Fiorentini M. L. (2013) Spatial variation in platinum group element concentrations in ore-bearing komatiite at the Long-Victor deposit, Kambalda Dome, Western Australia: enlarging the footprint of nickel sulfide orebodies. *Econ. Geol.* **108**, 913–933.

Bazarkina E. F., Pokrovski G. S. and Hazemann J.-L. (2014) Structure, stability and geochemical role of palladium chloride complexes in hydrothermal fluids. *Geochim. Cosmochim. Acta* **146**, 107–131.

Becke A. D. (1988) Density-functional exchange-energy approximation with correct asymptotic behavior. *Phys. Rev. A* **38**, 3098.

Becke A. D. (1993) Density functional thermochemisry: the role of exact exchange. *J. Chem. Phys.* **98**, 5648–5652.

Berendsen H. J. C., Grigera J. R. and Straatsma T. P. (1987) The missing term in effective pair potentials. *J. Phys. Chem.* **91**, 6269–6271.

Beret E. C., Pappalardo R. R., Doltsinis N. L., Marx D. and Sánchez Marcos E. (2008a) Aqueous PdII and PtII: anionic hydration revealed by Car–Parrinello simulations. *ChemPhysChem* **9**, 237–240.

Beret E. C., Martínez J. M., Pappalardo R. R., Marcos E. S., Doltsinis N. L. and Marx D. (2008b) Explaining asymmetric solvation of Pt(II) versus Pd(II) in aqueous solution revealed by *ab initio* molecular dynamics simulations. *J. Chem. Theory Comput.* **4**, 2108–2121.

Bethke C. M. (2008) *Geochemical and Biogeochemical Reaction Modeling*, second ed. Cambridge University Press, New York, p. 564.

Boily J.-F. and Seward T. M. (2005) Palladium (II) chloride complexation: Spectrophotometric investigation in aqueous solutions from 5 to 125 °C and theoretical insight into Pd–Cl and Pd–OH_2 interactions. *Geochim. Cosmochim. Acta* **69**, 3773–3789.

Boily J.-F., Seward T. M. and Charnock J. M. (2007) The hydrolysis and precipitation of Pd(II) in 0.6 mol•kg^{-1} NaCl: a potentiometric, spectrophotometric, and EXAFS study. *Geochim. Cosmochim. Acta* **71**, 4834–4845.

Boudreau A., Mathez E. and McCallum I. (1986) Halogen geochemistry of the Stillwater and Bushveld Complexes: evidence for transport of the platinum-group elements by Cl-rich fluids. *J. Petrol.* **27**, 967–986.

Bowron D. T., Beret E. C., Martin-Zamora E., Soper A. K. and Sánchez Marcos E. (2011) Axial structure of the Pd(II) aqua ion in solution. *J. Am. Chem. Soc.* **134**, 962–967.

Brugger J., Etschmann B., Liu W., Testemale D., Hazemann J. L., Emerich H., van Beek W. and Proux O. (2007) An XAS study of the structure and thermodynamics of Cu(I) chloride complexes in brines up to high temperature (400 °C, 600 bar). *Geochim. Cosmochim. Acta* **71**, 4920–4941.

Brugger J., Pring A., Reith F., Ryan C., Etschmann B., Liu W. H., O'Neill B. and Ngothai Y. (2010) Probing ore deposits formation: new insights and challenges from synchrotron and neutron studies. *Radiat. Phys. Chem.* **79**, 151–161.

Bühl M., Kabrede H., Diss R. and Wipff G. (2006) Effect of hydration on coordination properties of uranyl(VI) complexes. a first-principles molecular dynamics study. *J. Am. Chem. Soc.* **128**, 6357–6368.

Bühl M., Sieffert N., Golubnychiy V. and Wipff G. (2008) Density functional theory study of uranium(VI) aquo chloro complexes in aqueous solution. *J. Phys. Chem. A* **112**, 2428–2436.

Cabral A. R., Lehmann B., Tupinamba M., Schlosser S., Kwitko-Ribeiro R. and de Abreu F. R. (2009) The platiniferous Au–Pd belt of minas Gerais, Brazil, and genesis of its botryoidal Pt-Pd aggregates. *Econ. Geol.* **104**(8), 1265–1276.

Cabral A. R., Reith F., Lehmann B., Brugger J., Meinhold G., Tupinambá M. and Kwitko-Ribeiro R. (2012) Titanium mobility: insights from anatase nanoparticles on supergene platinum–palladium grains from Brazil. *Chem. Geol.* **334**, 182–188.

Campbell L., Rehr J. J., Schenter G. K., McCarthy M. I. and Dixon D. (1999) XAFS Debye–Waller factors in aqueous Cr^{+3} from molecular dynamics. *J. Synchrotron Radiat.* **6**, 310–312.

Car R. and Parrinello M. (1985) Unified approach for molecular dynamics and density-functional theory. *Phys. Rev. Lett.* **55**, 2471–2474.

Djon M. L. N. and Barnes S.-J. (2012) Changes in sulfides and platinum-group minerals with the degree of alteration in the Roby, Twilight, and High Grade Zones of the Lac des Iles Complex, Ontario, Canada. *Miner. Deposita* **47**, 875–896.

Driesner T. (2007) The system H_2O–NaCl. Part II: correlations for molar volume, enthalpy, and isobaric heat capacity from 0 to 1000 °C, 1 to 5000 bar, and 0 to 1 X_{NaCl}. *Geochim. Cosmochim. Acta* **71**, 4902–4919.

Driesner T. and Heinrich C. A. (2007) The system H_2O–NaCl. Part I: correlation formulae for phase relations in temperature–pressure–composition space from 0 to 1000 °C, 0 to 5000 bar, and 0 to 1 X_{NaCl}. *Geochim. Cosmochim. Acta* **71**, 4880–4901.

Etschmann B. E., Liu W., Testemale D., Müller H., Rae N. A., Proux O., Hazemann J. L. and Brugger J. (2010) An in situ XAS study of copper(I) transport as hydrosulfide complexes in hydrothermal solutions (25–592 °C, 180–600 bar): speciation and solubility in vapor and liquid phases. *Geochim. Cosmochim. Acta* **74**, 4723–4739.

Etschmann B. E., Black J., Grundler P., Borg S., Brewe D., McPhail D. C., Spiccia L. and Brugger J. (2011) Copper(I) speciation in mixed thiosulfate-chloride and ammonia-chloride solutions: XAS and UV–Visible spectroscopic studies. *RSC Adv.* **1**, 1554–1566.

Farrow C. E. and Watkinson D. H. (1996) Geochemical evolution of the epidote zone, Fraser mine, Sudbury, Ontario: Ni-Cu-PGE remobilization by saline fluids. *Explor. Min. Geol.* **5**, 17–31.

Fiorentini M. L., Barnes S. J., Lesher C. M., Heggie G. J., Keays R. R. and Burnham O. M. (2010) Platinum group element geochemistry of mineralized and nonmineralized komatiites and basalts. *Econ. Geol.* **105**, 795–823.

Gammons C. (1995) Experimental investigations of the hydrothermal geochemistry of platinum and palladium: IV. The stoichiometry of Pt (IV) and Pd (II) chloride complexes at 100 to 300 °C. *Geochim. Cosmochim. Acta* **59**, 1655–1667.

Gammons C. and Bloom M. (1993) Experimental investigation of the hydrothermal geochemistry of platinum and palladium: II. The solubility of PtS and PdS in aqueous sulfide solutions to 300 °C. *Geochim. Cosmochim. Acta* **57**, 2451–2467.

Gammons C., Bloom M. and Yu Y. (1992) Experimental investigation of the hydrothermal geochemistry of platinum and palladium: I. Solubility of platinum and palladium sulfide minerals in NaCl/H_2SO_4 solutions at 300° C. *Geochim. Cosmochim. Acta* **56**, 3881–3894.

Gammons C., Yu Y. and Bloom M. (1993) Experimental investigation of the hydrothermal geochemistry of platinum and palladium: III. The solubility of Ag–Pd alloy + AgCl in NaCl/HCl solutions at 300 °C. *Geochim. Cosmochim. Acta* **57**, 2469–2479.

Hester J. R., Maslen E. N., Spadaccini N., Ishizawa N. and Satow Y. (1993) Electron-density in potassium tetrachloropalladate (K_2PdCl_4) from synchrotron-radiation data. *Acta Cryst.* **B49**, 842–846.

Head-Gordon M., Pople J. A. and Frisch M. J. (1988) MP2 energy evaluation by direct methods. *Chem. Phys. Lett.* **153**, 503–506.

UNCORRECTED PROOF

Please cite this article in press as: Mei Y., et al. Palladium complexation in chloride- and bisulfide-rich fluids: Insights from *ab initio* molecular dynamics simulations and X-ray absorption spectroscopy. *Geochim. Cosmochim. Acta* (2015), http://dx.doi.org/10.1016/j.gca.2015.04.009

Hofer T. S., Randolf B. R., Adnan Ali Shah S., Rode B. M. and Persson I. (2007) Structure and dynamics of the hydrated palladium(II) ion in aqueous solution A QMCF MD simulation and EXAFS spectroscopic study. *Chem. Phys. Lett.* **445**, 193–197.

Hoffmann M. M., Darab J. G., Palmer B. J. and Fulton J. L. (1999) A transition in the Ni^{2+} complex structure from six- to four-coordinate upon formation of ion pair species in supercritical water: an X-ray absorption fine structure, near-infrared, and molecular dynamics study. *J. Phys. Chem.* **103**(42), 8471–8482.

Hsu L., Lechler P. J. and Nelson J. H. (1991) Hydrothermal solubility of palladium in chloride solutions from 300 degrees to 700 °C; preliminary experimental results. *Econ. Geol.* **86**, 422–427.

Joly Y. (2001) X-ray absorption near-edge structure calculations beyond the muffin-tin approximation. *Phys. Rev. B* **63**, 125120.

Keays R. R. and Davison R. (1976) Palladium, iridium, and gold in the ores and host rocks of nickel sulfide deposits in Western Australia. *Econ. Geol.* **71**, 1214–1228.

Le Vaillant M., Barnes S. J., Miller J., McCuaig T. C., Mucilli P. and Fiorentini M. L. (2014) A hydrothermal Ni-As-PGE geochemical halo around the Miitel nickel sulfide deposit, Yilgarn Craton, Western Australia. *Econ. Geol.* **110**, 505–530.

Lee C., Yang W. and Parr R. G. (1988) Development of the Colle-Salvetti correlation-energy formula into a functional of the electron density. *Phys. Rev. B* **37**, 785.

Lemmon E. W., Jacobsen R. T., Penoncello S. G. and Friend D. G. (2000) Thermodynamic properties of air and mixtures of nitrogen, argon, and oxygen from 60 to 2000 K at pressures to 2000 MPa. *J. Phys. Chem. Ref. Data* **29**, 331–385.

Lin I. C., Seitsonen A. P., Tavernelli I. and Rothlisberger U. (2012) Structure and dynamics of liquid water from ab initio molecular dynamics—comparison of BLYP, PBE, and revPBE density Functionals with and without van der Waals corrections. *J. Chem. Theory Comput.* **8**, 3902–3910.

Liu W., Borg S., Etschmann B., Mei Y. and Brugger J. (2012) An XAS study of speciation and thermodynamic properties of aqueous zinc bromide complexes at 25–150 °C. *Chem. Geol.* **298–299**, 57–69.

Liu W., Borg S., Testemale D., Etschmann B., Hazemann J.-L. and Brugger J. (2011) Speciation and thermodynamic properties for cobalt chloride complexes in hydrothermal fluids at 25–400 °C and 600 bar: an in-situ XAS study. *Geochim. Cosmochim. Acta* **75**, 1227–1248.

Liu W., Etschmann B., Testemale D., Hazemann J.-L., Rempel K., Müller H. and Brugger J. (2014) Gold transport in hydrothermal fluids: competition among the Cl^-, Br^-, HS^- and NH_3(aq) ligands. *Chem. Geol.* **376**, 11–19.

Locmelis M., Fiorentini M. L., Barnes S. J. and Pearson N. J. (2013) Ruthenium variation in chromite from komatiites and komatiitic basalts—a potential mineralogical indicator for nickel sulfide mineralization. *Econ. Geol.* **108**, 355-36.

Martínez J. M., Torrico F., Pappalardo R. R. and Sánchez Marcos E. (2004) Understanding the hydration structure of square-planar aquaions: the $[Pd(H_2O)_4]^{2+}$ case. *J. Phys. Chem. B* **108**, 15851–15855.

Mason W. R. and Gray H. B. (1968) Electronic structures of square-planar complexes. *J. Am. Chem. Soc.* **90**, 5721–5729.

Mei Y., Sherman D. M., Liu W. and Brugger J. (2013a) *Ab initio* molecular dynamics simulation and free energy exploration of copper(I) complexation by chloride and bisulfide in hydrothermal fluids. *Geochim. Cosmochim. Acta* **102**, 45–64.

Mei Y., Sherman D. M., Liu W. and Brugger J. (2013b) Complexation of gold in S3–rich hydrothermal fluids: evidence from ab initio molecular dynamics simulations. *Chem. Geol.* **347**, 34–42.

Mei Y., Liu W., Sherman D. M. and Brugger J. (2014) Metal complexation and ion hydration in low density hydrothermal fluids: ab initio molecular dynamics simulation of Cu(I) and Au(I) in chloride solutions (25–1000 °C, 1–5000 bar). *Geochim. Cosmochim. Acta* **131**, 196–212.

Mei Y., Sherman D., Liu W., Etschmann B., Testemale D. and Brugger J. (2015) Zinc complexation in chloride-rich hydrothermal fluids (25 to 600 °C): a thermodynamic model derived from ab initio molecular dynamics. *Geochim. Cosmochim. Acta* **150**, 265–284.

Mernagh T. P., Heinrich C. A., Leckie J. F., Carville D. P., Gilbert D. J., Valenta R. K. and Wyborn L. A. I. (1994) Chemistry of low-temperature hydrothermal gold, platinum, and palladium (±uranium) mineralization at Coronation Hill, Northern Territory, Australia. *Econ. Geol.* **89**, 1053–1073.

Pan P. and Wood S. (1994) Solubility of Pt and Pd sulfides and Au metal in aqueous bisulfide solutions. *Miner. Deposita* **29**, 373–390.

Proux O., Biquard X., Lahera E., Menthonnex J. J., Prat A., Ulrich O., Soldo Y., Trevisson P., Kapoujyan G., Perroux G., Taunier P., Grand D., Jeantet P., Deleglise M., Roux J. P. and Hazemann J. L. (2005a) FAME: a new beamline for X-ray absorption investigations of very diluted systems of environmental, material and biological interests. *Phys. Scr.* **T115**, 970–973.

Proux O., Nassif V., Prat A., Ulrich O., Lahera E., Biquard X., Menthonnex J.-J. and Hazemann J.-L. (2005b) Feedback system of a liquid-nitrogen-cooled double-crystal monochromator: design and performances. *J. Synchrotron Radiat.* **13**, 59–68.

Ravel B. and Newville M. (2005) ATHENA, ARTEMIS, HEPHAESTUS: data analysis for X-ray absorption spectroscopy using IFEFFIT. *J. Synchrotron Radiat.* **12**, 537–541.

Rehr J. J., Kas J. J., Vila F. D., Prange M. P. and Jorissen K. (2010) Parameter-free calculations of X-ray spectra with FEFF9. *Phys. Chem. Chem. Phys.* **12**, 5503–5513.

Resat H. M. and Mihaly (1993) Studies on free energy calculations. I. Thermodynamic integration using a polynomial path. *J. Chem. Phys.* **99**, 6052–6061.

Sassani D. C. and Shock E. L. (1990) Speciation and solubility of palladium in aqueous magmatic-hydrothermal solutions. *Geology* **18**, 925–928.

Sassani D. C. and Shock E. L. (1998) Solubility and transport of platinum-group elements in supercritical fluids: summary and estimates of thermodynamic properties for ruthenium, rhodium, palladium, and platinum solids, aqueous ions, and complexes to 1000 °C and 5 kbar. *Geochim. Cosmochim. Acta* **62**, 2643–2671.

Seward T. M. and Barnes H. L. (1997) Metal transport in hydrothermal ore fluids. In *Geochemistry of Hydrothermal Ore Deposits* (ed. H. L. Barnes), third ed. John-Wiley and Sons, New York, pp. 435–486.

Seward T. M. and Driesner T. (2004) Hydrothermal solution structure: experiments and computer simulations. In *Aqueous Systems at Elevated Temperatures and Pressures: Physical Chemistry in Water, Steam and Hydrothermal Solutions* (eds. D. A. Palmer, R. Fernández-Prini and A. H. Havey). Elsevier, pp. 149–182.

Seward T. M., Henderson C. M. B. and Charnock J. M. (2002) An Exafs study of Pd^{2+} solvation in aqueous media and chloride complexing to 340 °C at saturated vapour pressure. *Geochim. Cosmochim. Acta* **66**, A699.

Sharps J. A., Brown, Jr, G. E. and Stebbins J. F. (1993) Kinetics and mechanism of ligand exchange of Au (III), Zn(II), and Cd(II) chlorides in aqueous solution: an NMR study from 28–98 °C. *Geochim. Cosmochim. Acta* **57**, 721–731.

UNCORRECTED PROOF

Please cite this article in press as: Mei Y., et al. Palladium complexation in chloride- and bisulfide-rich fluids: Insights from *ab initio* molecular dynamics simulations and X-ray absorption spectroscopy. *Geochim. Cosmochim. Acta* (2015), http://dx.doi.org/10.1016/j.gca.2015.04.009

Sherman D. M. (2007) Complexation of Cu^{+} in Hydrothermal NaCl Brines: *Ab initio* molecular dynamics and energetics. *Geochim. Cosmochim. Acta* **71**, 714–722.

Shvarov Y. (2008) HCh: new potentialities for the thermodynamic simulation of geochemical systems offered by windows. *Geochem. Int.* **46**, 834–839.

Shvarov Y. V. and Bastrakov E. (1999) *HCh: A Software Package for Geochemical Equilibrium Modelling. User's Guide Record/25*. Australian Geological Survey Organisation, Canberra.

Smith D. E. and Dang L. X. (1994) Computer simulations of NaCl association in polarizable water. *J. Chem. Phys.* **100**, 3757–3766.

Sprik M. and Ciccotti G. (1998) Free energy from constrained molecular dynamics. *J. Chem. Phys.* **109**, 7737–7744.

Susak N. J. and Crerar D. A. (1985) Spectra and coordination changes of transition metals in hydrothermal solutions: implications for ore genesis. *Geochim. Cosmochim. Acta* **49**, 555–564.

Tagirov B. and Baranova N. (2009) The state of palladium in sulfide hydrothermal solutions: experimental solubility study. *Geochem. Int.* **47**, 1234–1242.

Tagirov B. R., Baranova N. N., Zotov A. V., Akinfiev N. N., Polotnyanko N. A., Shikina N. D., Koroleva L. A., Shvarov Y. V. and Bastrakov E. N. (2013) The speciation and transport of palladium in hydrothermal fluids: experimental modeling and thermodynamic constraints. *Geochim. Cosmochim. Acta* **117**, 348–373.

Testemale D., Argoud R., Geaymond O. and Hazemann J. L. (2005) High pressure/high temperature cell for X-ray absorption and scattering techniques. *Rev. Sci. Instrum.* **76**, 043905.

Tian Y., Etschmann B., Testemale D., Ngothai Y. and Brugger J. (2014) Speciation and thermodynamic properties of manganese(II) chloride complexes in hydrothermal fluids: *in situ* XAS and quantum-chemical study. *Geochim. Cosmochim. Acta* **129C**, 77–95.

Tooth B., Ciobanu C. L., Green L., O'Neill B. and Brugger J. (2011) Bi-melt formation and gold scavenging from hydrothermal fluids: an experimental study. *Geochim. Cosmochim. Acta* **75**, 5423–5443.

Tooth B., Etschmann B., Pokrovski G. S., Testemale D., Hazemann J. L., Grundler P. V. and Brugger J. (2013) Bismuth speciation in hydrothermal fluids: an X-ray absorption spectroscopy and solubility study. *Geochim. Cosmochim. Acta* **101**, 156–172.

Troullier N. and Martins J. L. (1991) Efficient pseudopotentials for plane-wave calculations. *Phys. Rev. B* **43**, 1993.

Usher A., McPhail D. C. and Brugger J. (2009) A spectrophotometric study of aqueous Au(III)-halide-hydroxy complexes at 25 °C. *Geochim. Cosmochim. Acta* **73**, 3359–3380.

Willmore C. C., Boudreau A. E. and Kruger F. J. (2000) The halogen geochemistry of the Bushveld Complex, Republic of South Africa: implications for chalcophile element distribution in the lower and critical zones. *J. Petrol.* **41**, 1517–1539.

Wood S. (2002) The aqueous geochemistry of the platinum-group elements with applications to ore deposits. In *The Geology, Geochemistry, Mineralogy and Mineral Beneficiation of Platinum-Group Elements*, SV 54, pp. 211–249. The Geology, Geochemistry, Mineralogy and Mineral Beneficiation of Platinum-Group Elements. CIM.

Wood S. A. and Mountain B. W. (1991) Hydrothermal solubility of palladium in chloride solutions from 300 degrees to 700 degrees C; preliminary experimental results; discussion. *Econ. Geol.* **86**, 1562–1563.

Wood S. A., Mountain B. W. and Fenlon B. J. (1989) Thermodynamic constraints on the solubility of platinum and palladium in hydrothermal solutions; reassessment of hydroxide, bisulfide, and ammonia complexing. *Econ. Geol.* **84**, 2020–2028.

Wood S. A., Mountain B. W. and Pan P. (1992) The aqueous geochemistry of platinum, palladium and gold; recent experimental constraints and a re-evaluation of theoretical predictions. *Can. Mineral.* **30**, 955–982.

Vanquickenborne L. G. and Ceulemans A. (1981) Ligand field spectra of square-planar platinum(II) and palladium(II) complexes. *Inorg. Chem.* **20**, 796–800.

Vidossich P., Ortuño M. Á., Ujaque G. and Lledós A. (2011) Do metal water hydrogen bonds hold in solution? Insight from *ab initio* molecular dynamics simulations. *ChemPhysChem* **12**, 1666–1668.

Xiong Y. and Wood S. (2000) Experimental quantification of hydrothermal solubility of platinum-group elements with special reference to porphyry copper environments. *Mineral. Petrol.* **68**, 1–28.

Associate editor: Jean Francois Boily

UNCORRECTED PROOF